Steel Corrosion Mechanisms during Pipeline Operation: In-Situ Characterization

Claire Chisholm, William Mook, Dan Bufford, Khalid Hattar, and Katherine Jungjohann

Sandia National Laboratories, New Mexico

Steven Hayden, Timothy Kucharski, Tatiana Pilyugina, Rachael Grudt, and Michele Ostraat

Aramco Services Company, Aramco Research Center, Boston, MA

This work was performed at the Center for Integrated Nanotechnologies (CINT), an Office of Science User Facility operated for the U.S. Department of Energy (DOE) Office of Science. Sandia National Laboratories is a multi-program laboratory managed and operated by Sandia Corporation, a wholly owned subsidiary of Lockheed Martin Corporation, for the U.S. Department of Energy's National Nuclear Security Administration under contract DE-AC04-94AL85000.

Global problem

annual US corrosion costs $276,000,000,000 $ 276 B

3.1% US GDP lost to corrosion

investing in controls | dealing with failures

US corrosion costs breakdown

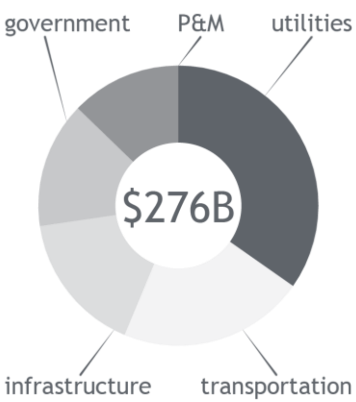

electrical utilities
gas distribution
drinking water
sewers

bridges
railroads
airports
ports

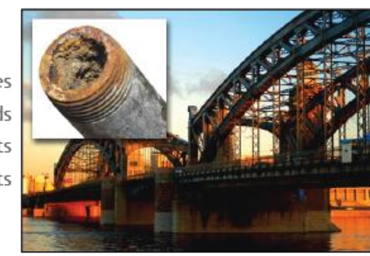

ships
aircraft
motor vehicles
railroad cars

oil & gas pipelines
petroleum refining
mining
chemical/pharma

Pipeline Steel Corrosion: Oil and Gas Extraction

annual US corrosion costs $276,000,000,000 $ 276 B

3.1% US GDP lost to corrosion
investing in controls | dealing with failures

Steel failure caused by local corrosion, pitting, and eventual cracking

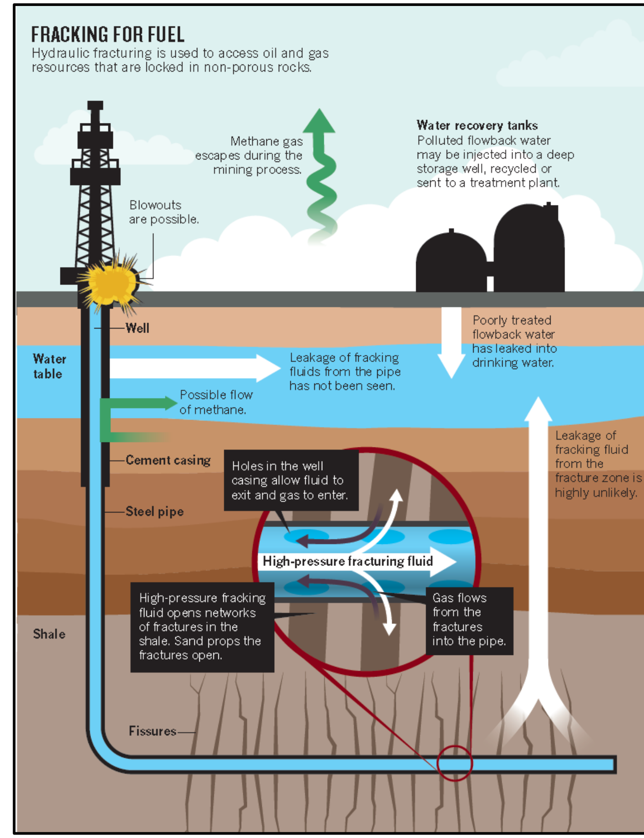

Howarth et al., Nature **477**, 271 (2011)

Mechanisms for pipeline corrosion initiation are unclear

- Grain boundaries are highly susceptible to corrosion in atm environments
- Cementite acts as a cathode, while Fe dissolution occurs in ferrite or pearlite structures, deviation of 10-20 mV between ferrite and cementite (Bai et al, 2015)
- Surface film peeling exposes new surfaces to continue corrosion

Structure & Composition of 1018 Carbon Steel

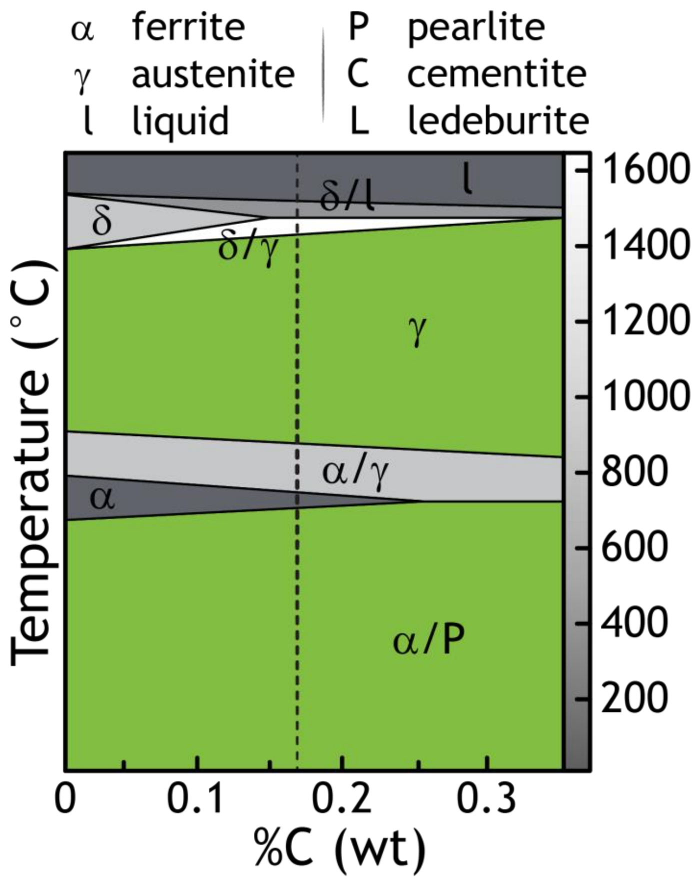

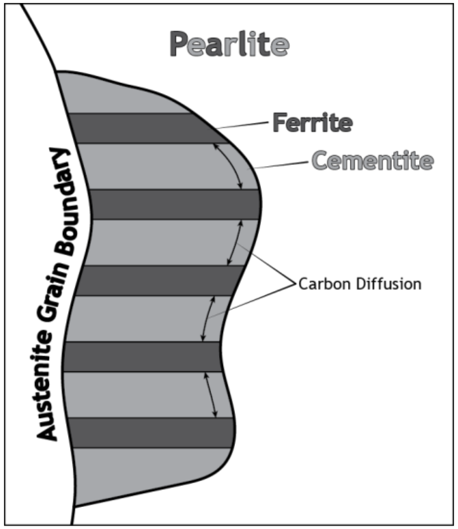

Pearlite: alternating layers of ferrite (88 wt%) and cementite (12 wt%)

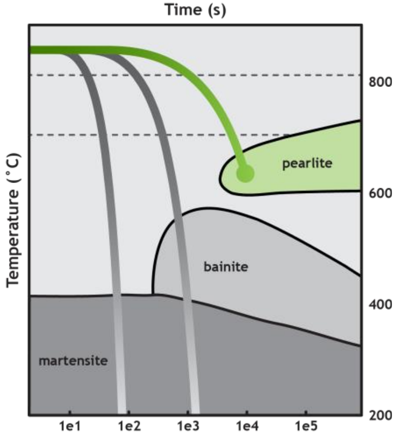

Element	Mass %
Fe	98.305
C	0.160
Mn	0.710
Cu	0.345
Si	0.169
Cr	0.116
Ni	0.107

- 1018 is forged from 1150 – 1280 °C down to a temperature in the area of 600 – 650 °C

Pipeline Steel Corrosion: Sweet Corrosion CO_2

Water reacts with dissolved CO_2 to form carbonic acid
Corrosion rate dependent on partial pressure of CO_2 and temperature (affects surface film that is formed)
Protective scale: iron carbonate films form, $FeCO_3$
Water composition effects the buffering capacity

Determinant Parameters:

- Solution composition: pH, wetting, phase ratios
- Salt composition (NaCl, K^+, Ca^{2+}) and concentrations
- CO_2 content
- Temperature & Pressure
- Steel surface: corrosion film, protective molecules
- Fluid dynamics, flow rate (mass transport of CO_2)
- Steel composition

Partnership with ASC to tackle corrosion problem

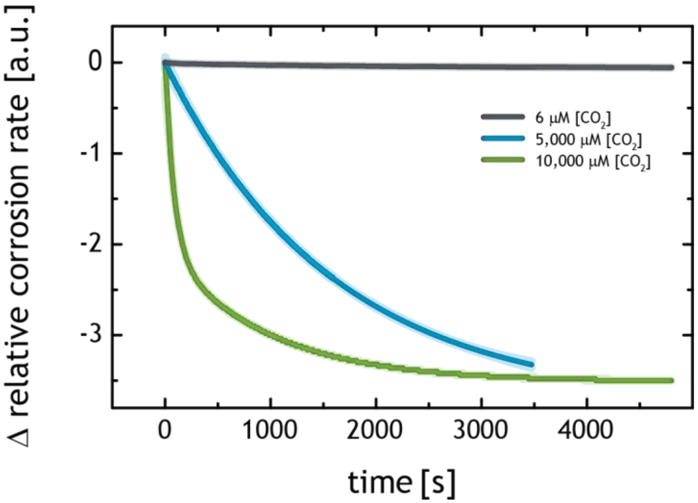

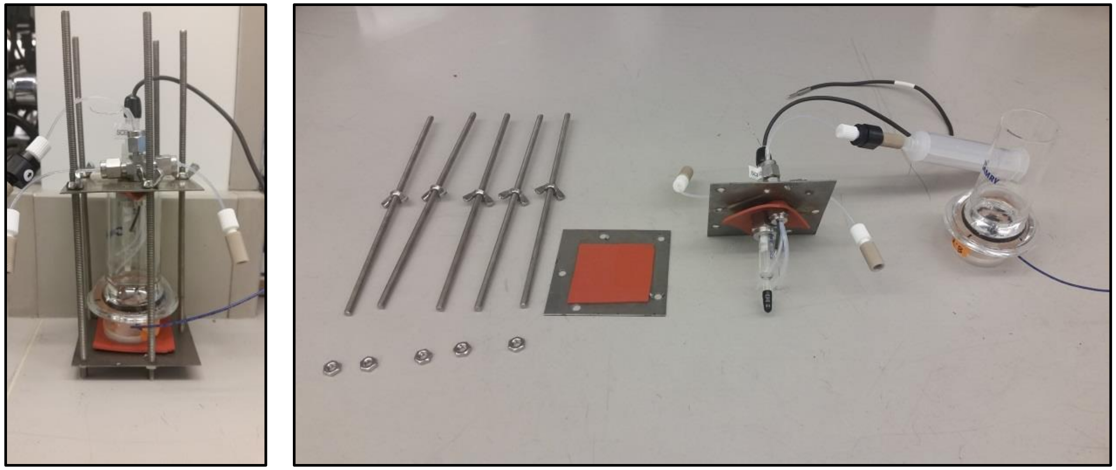

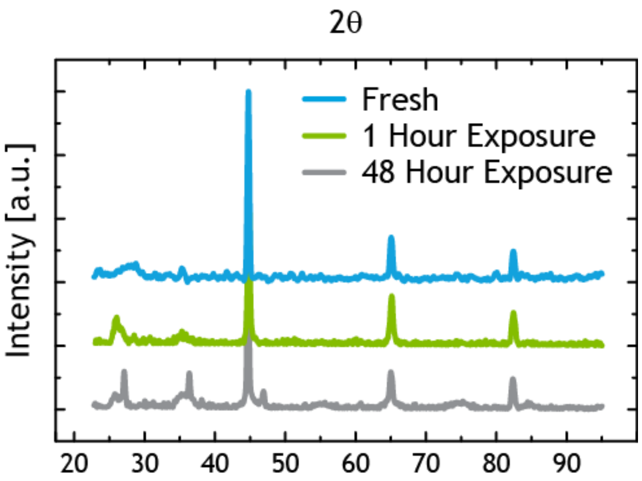

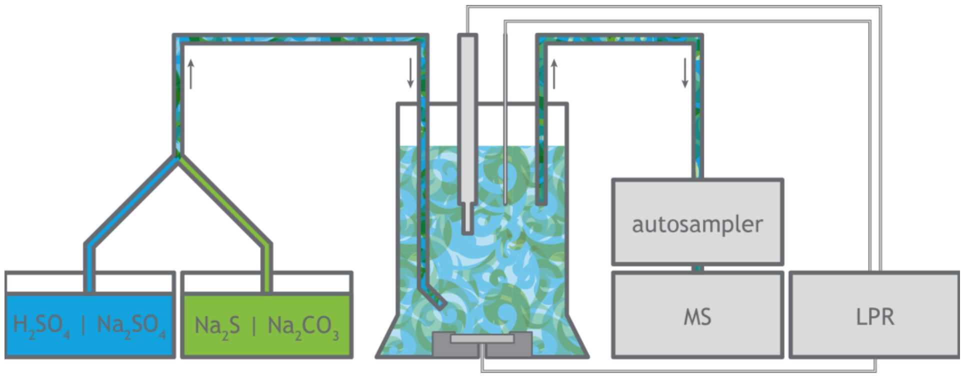

Corrosion Initiates at Grain Boundaries

Which grain boundaries? Nanoscale sites?

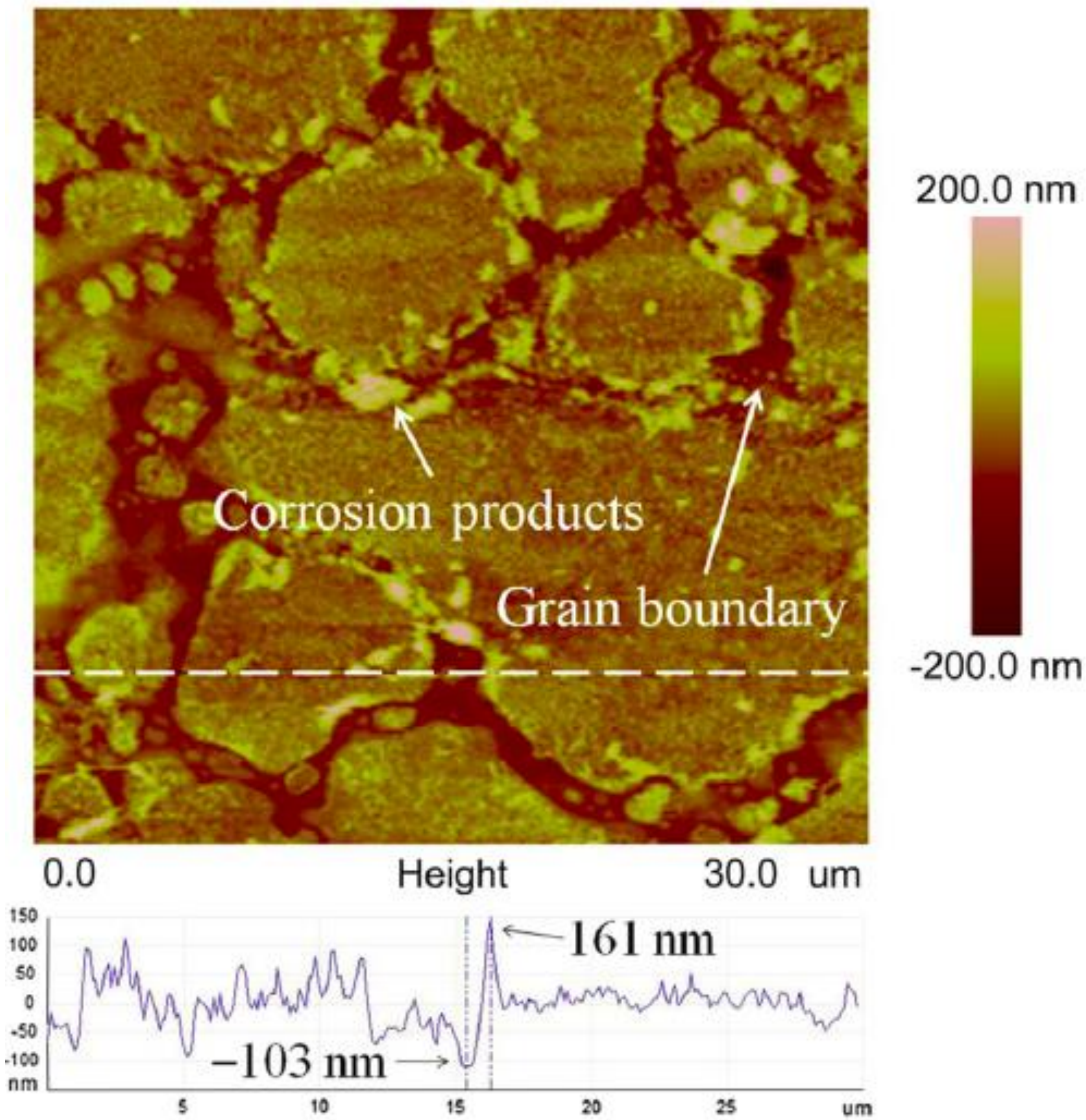

Bai et al., 2015 Corr. Sci. **93**, 109-119.

In-situ TEM Ideally Suited for Nanoscale Corrosion

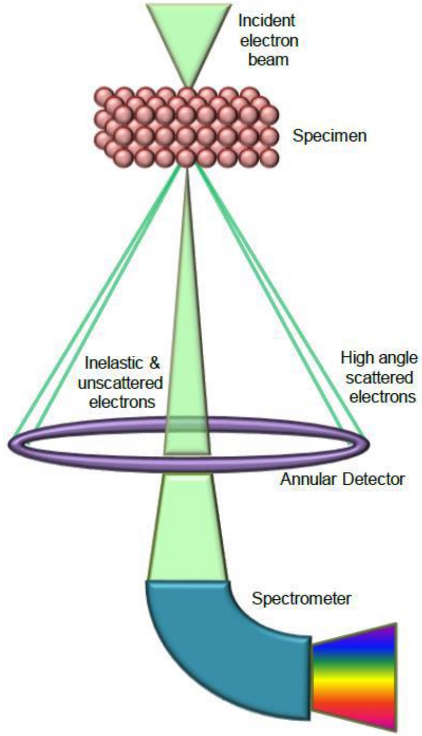

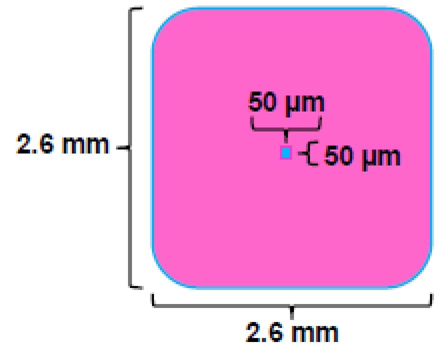

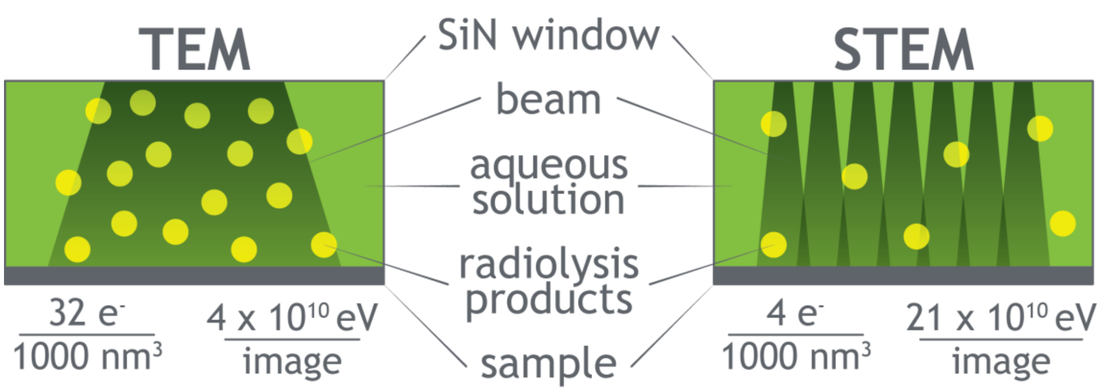

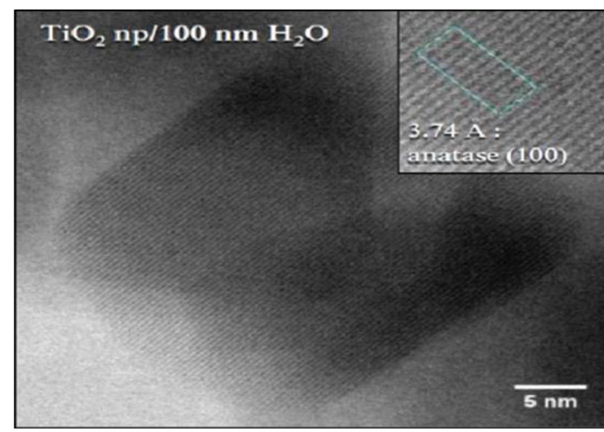

Electron Beam Radiolysis of Aqueous Media

$$H_2O \rightsquigarrow 0.28\ e_{aq}^{-},\ 0.062\ H^{\cdot},\ 0.28\ {}^{\cdot}OH,\ 0.047\ H_2,\ 0.073\ H_2O_2,\ 0.28\ \mu mol\ J^{-1}$$

Buxton, VCH Weinheim (1987)

*Amount of products formed depends on the electron dose

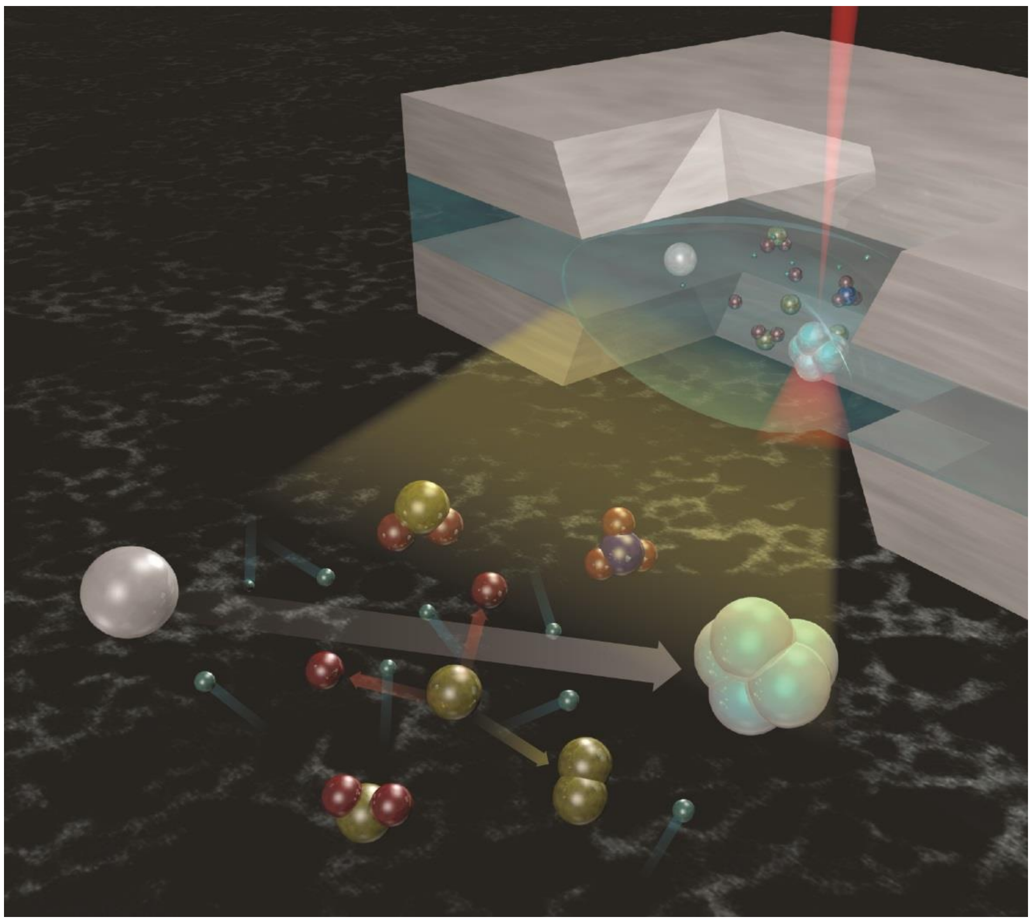

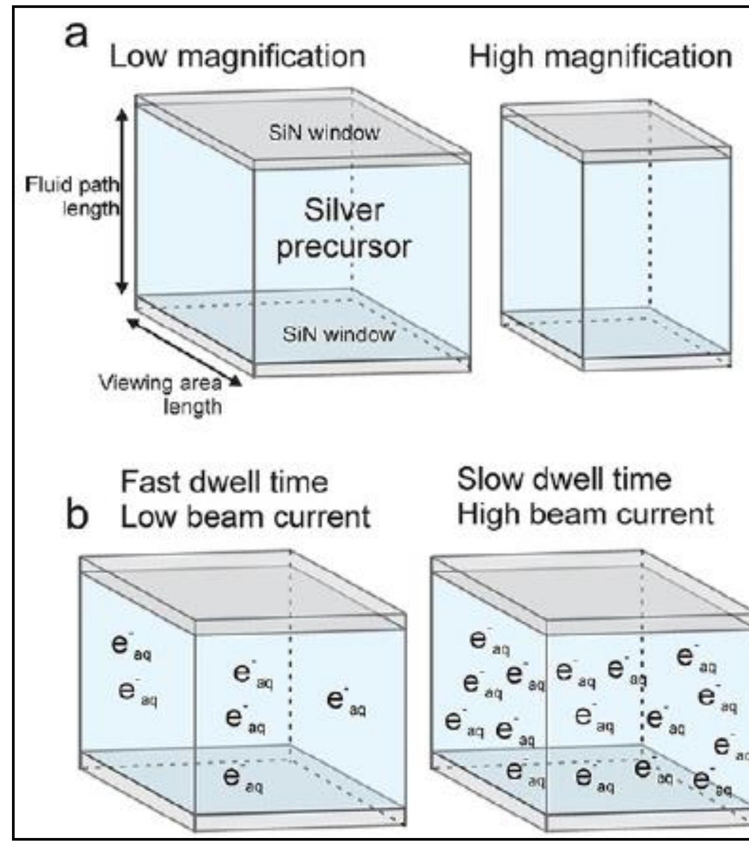

Woehl et al. ACS Nano **6**, 8599 (2012).

Sample Preparation and Screening

1. Deposit protective Pt layer
2. Trench into low-carbon steel
3. U-cut
4. Attach to micromanipulator
5. Transfer to TEM grid
6. 3 step thinning process
7. Precession Electron Diffraction mapping
8. Transfer to SiN membrane chip for corrosion experiment
9. Load sample in Hummingbird Scientific Liquid Cell TEM holder with DI water between top and bottom chip.
10. Prefill intake line with DI water.

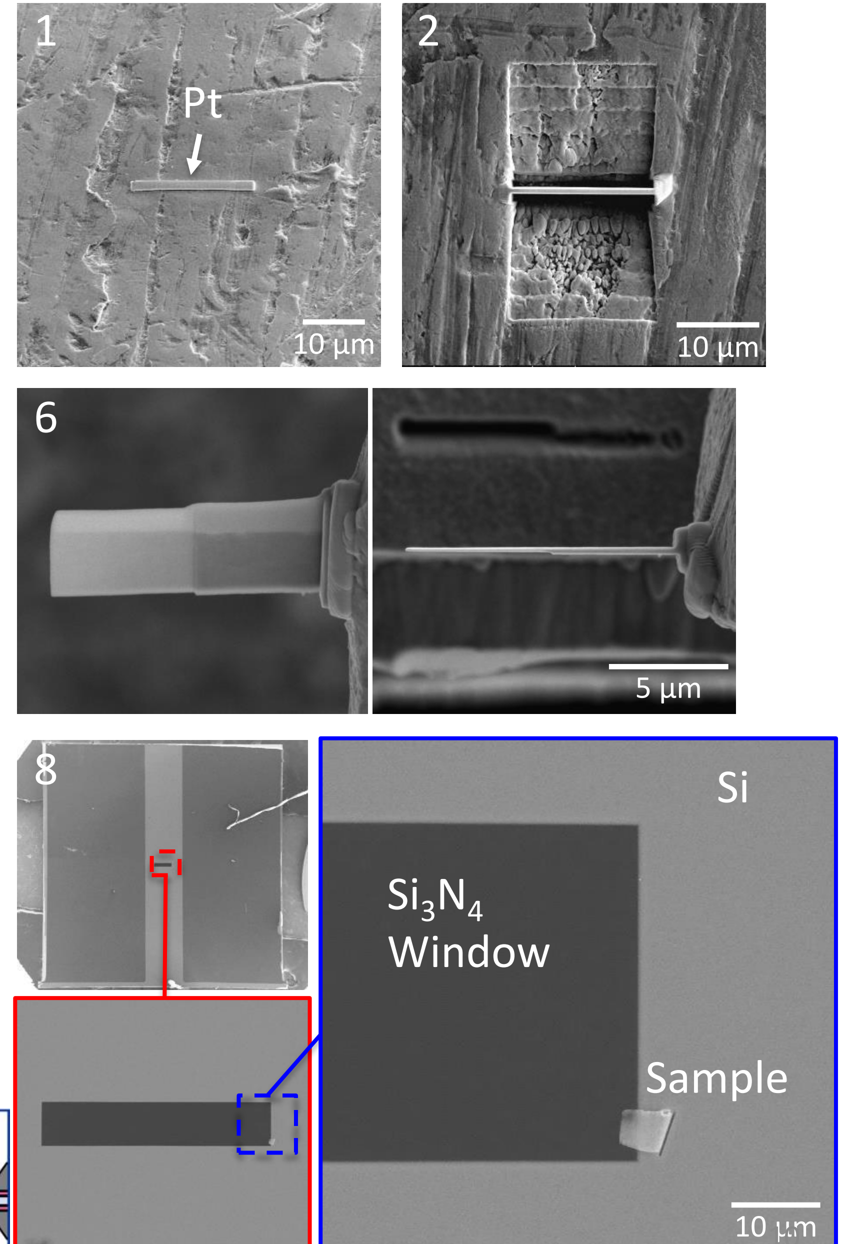

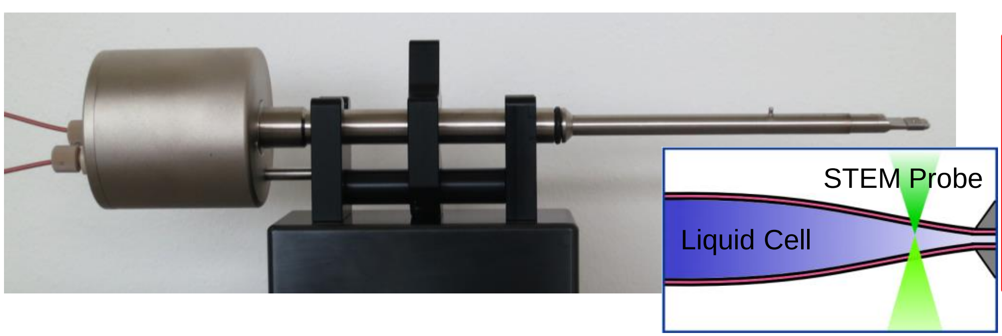

Focused Ion Beam Sample Preparation

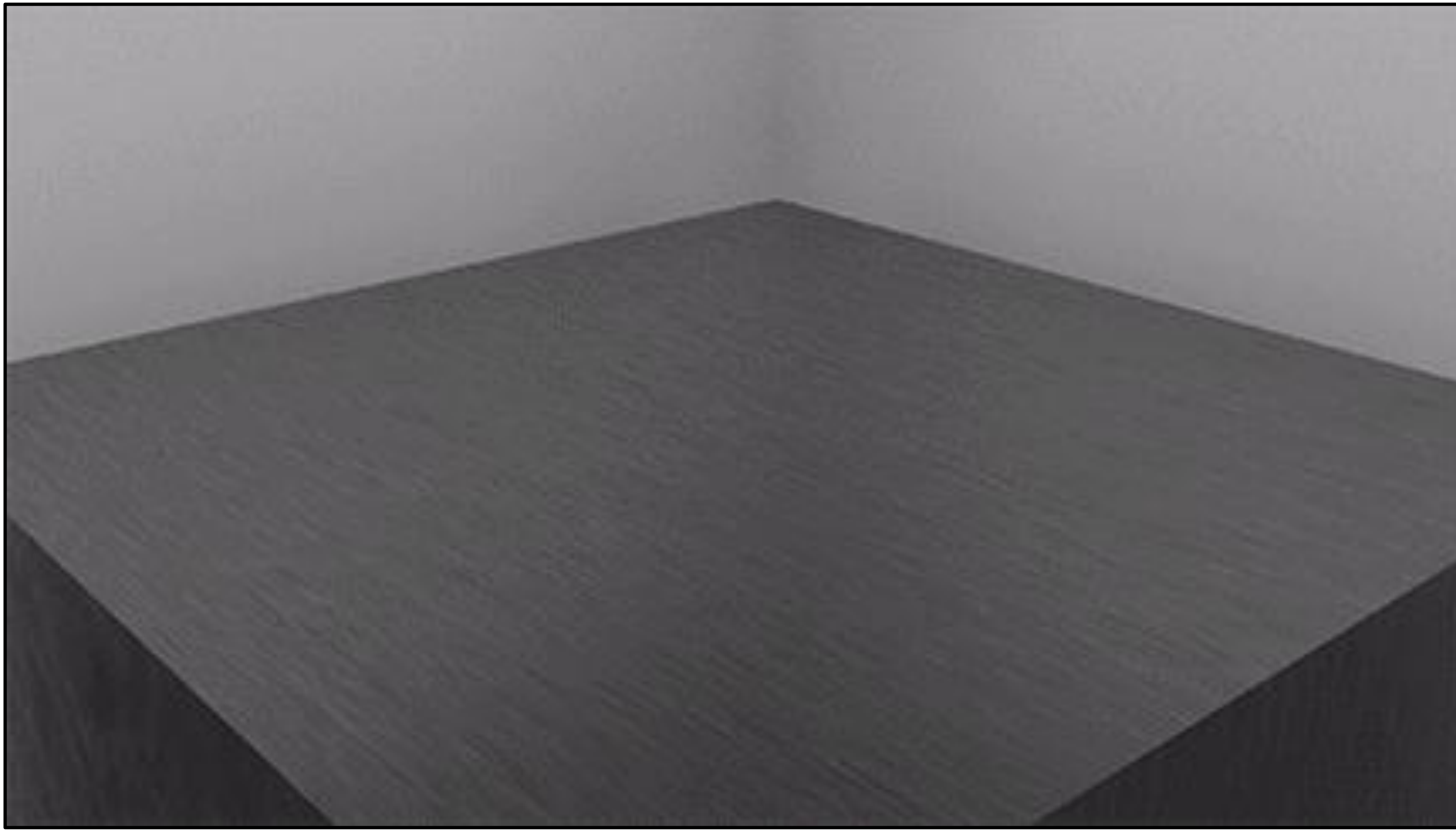

Low-Carbon Steel Microstructure

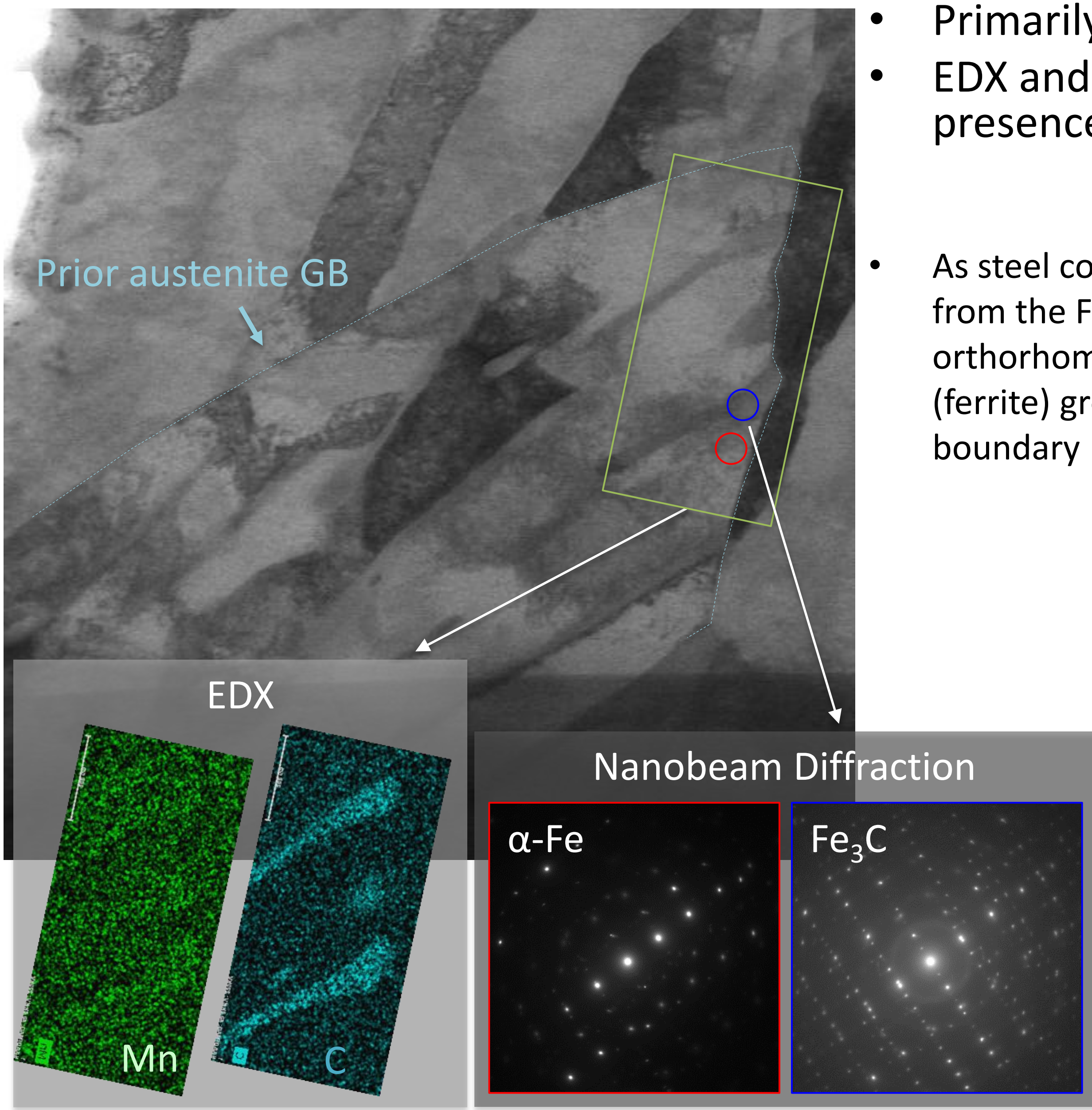

- Primarily BCC α-Fe
- EDX and nanobeam diffraction show presence of Mn-rich Fe_3C lamellae

- As steel cools past the eutectic temperature from the FCC γ-Fe (austenite) phase, orthorhombic Fe_3C (cementite) and BCC α-Fe (ferrite) grow, starting at a prior austenite grain boundary

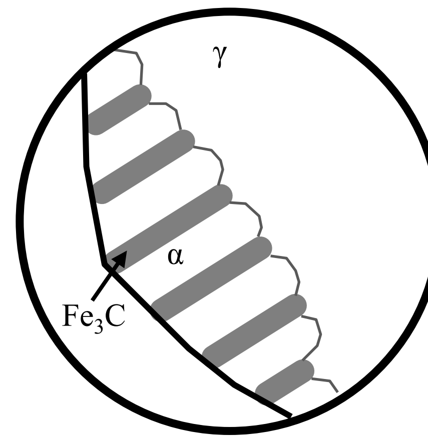

Grain Orientation Mapping of BCC Ferrite

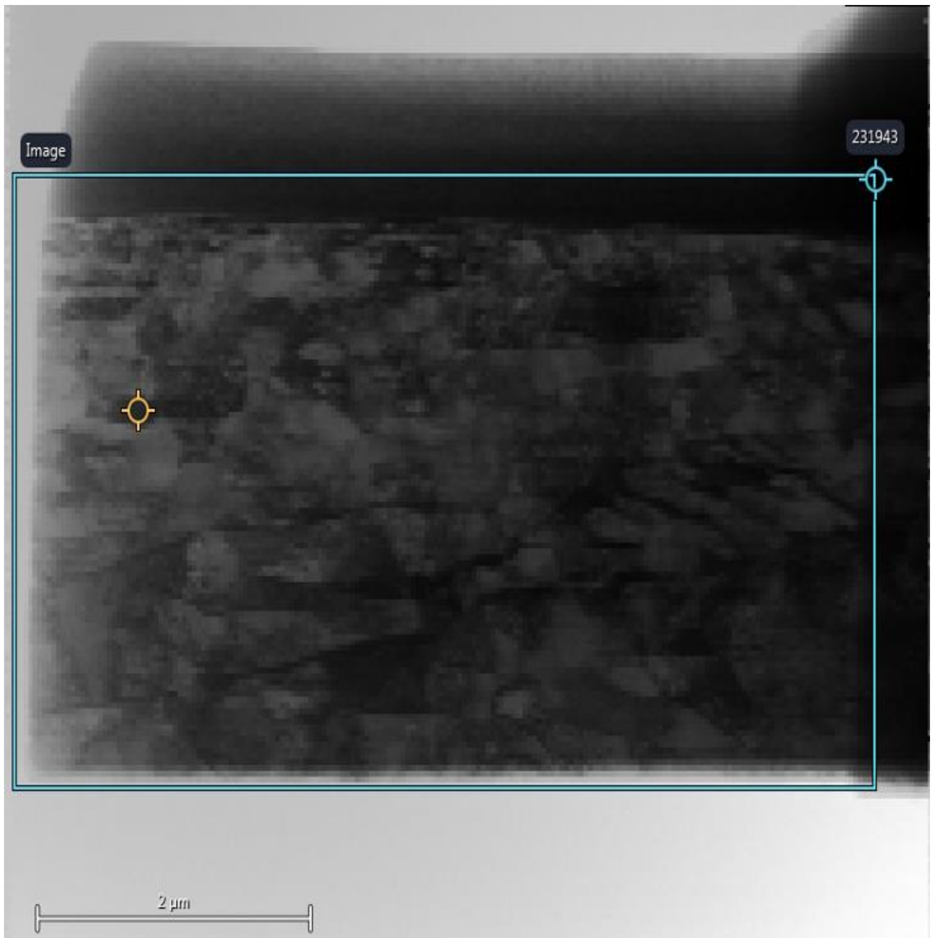

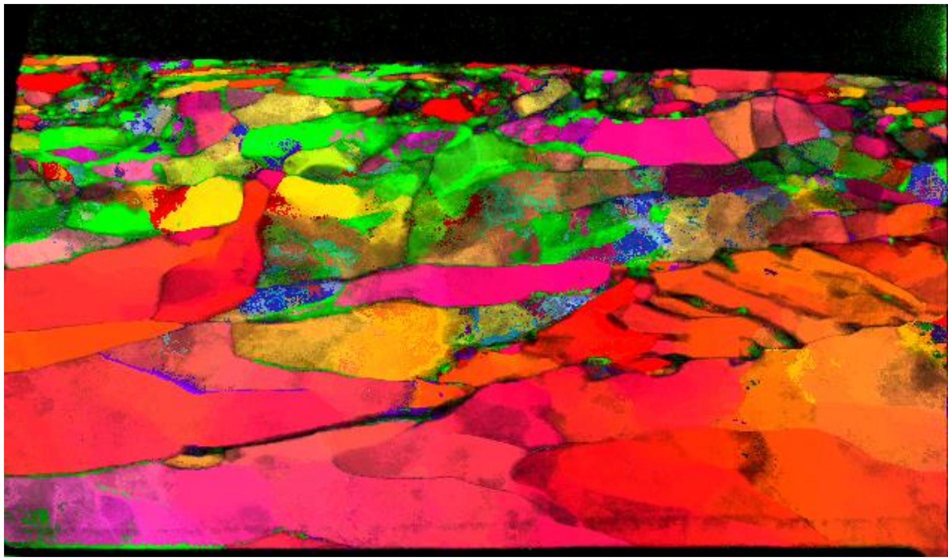

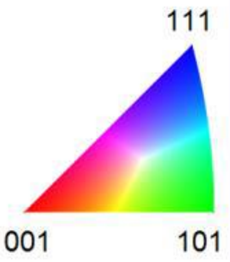

10 nm step size across thinned sample region,
only thin region is placed on SiN membrane window

Low-Carbon Steel in 0.27 ppm CO_2:
Microstructural Evolution Overview

- Overall thinning
- Black arrow
  - Edge corrosion
- White arrow
  - Internal grain preferential etching
- White box
  - Preferential α-Fe etching (over Fe_3C)

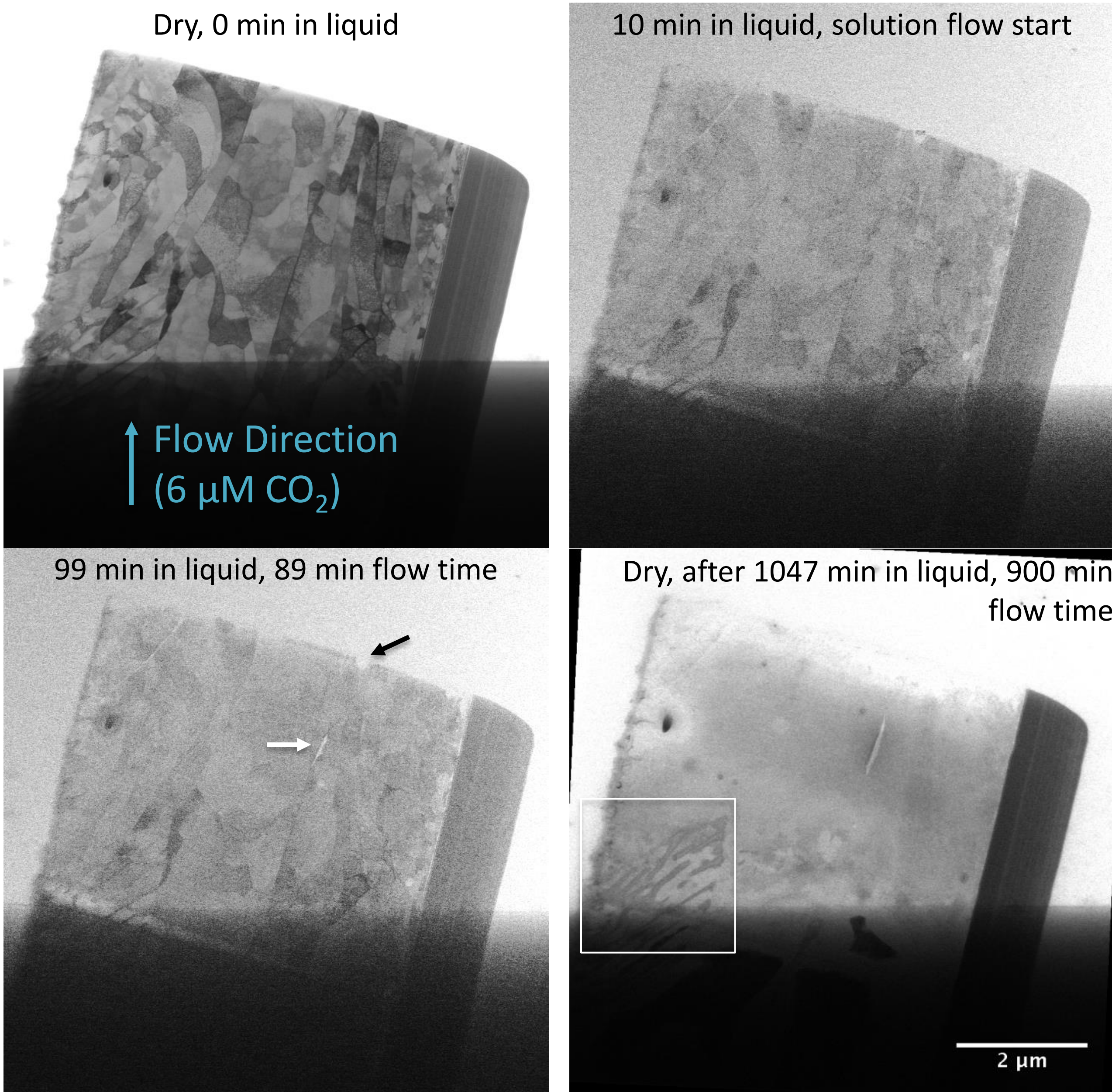

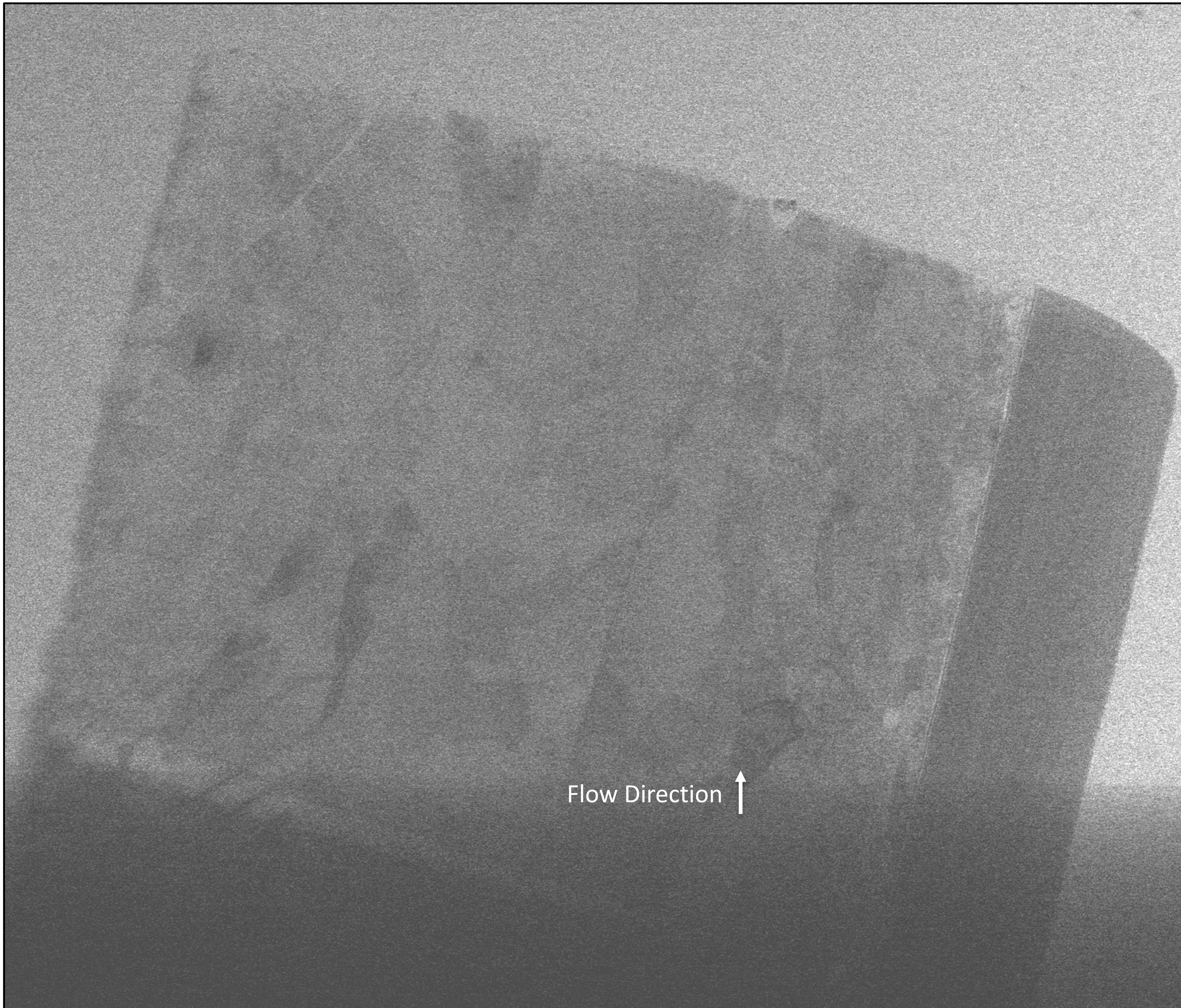
Flow Direction

Edge Corrosion of Steel in 0.27 ppm CO_2

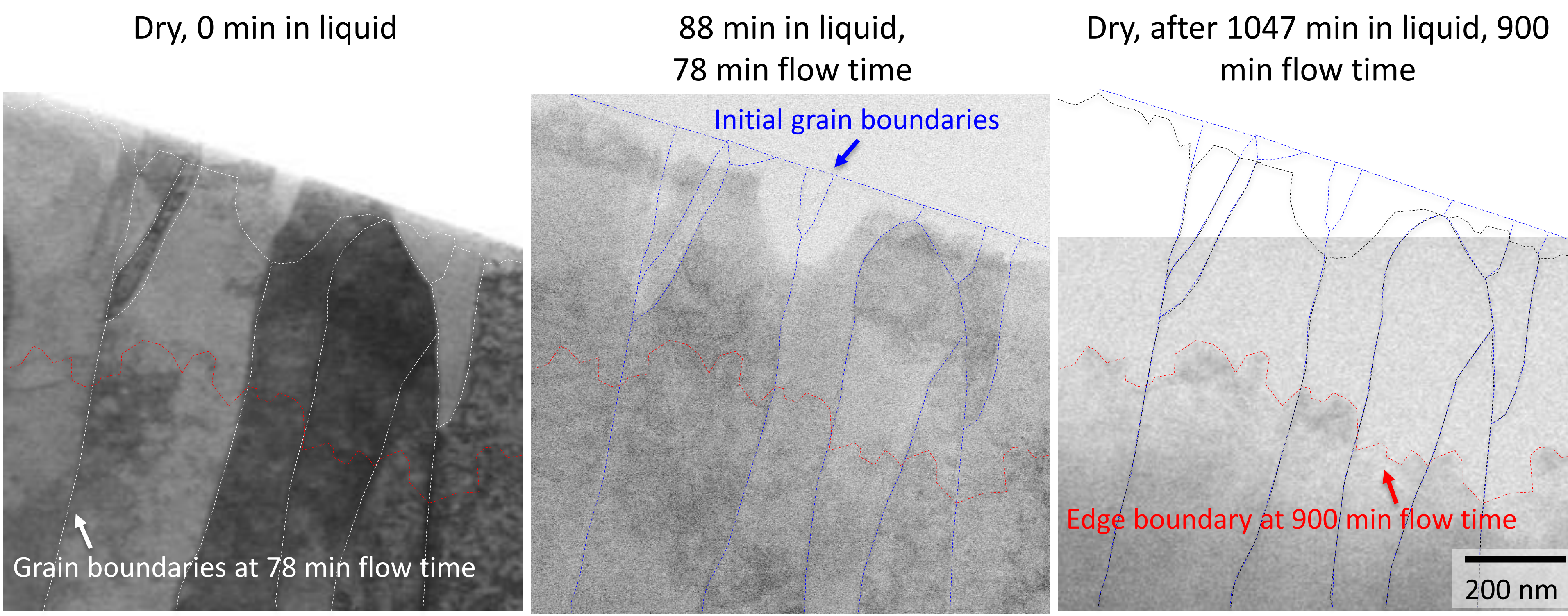

- Initial preferential etching in some areas
- Overall slight etching preference at grain boundaries
- Eventual non-selective etching

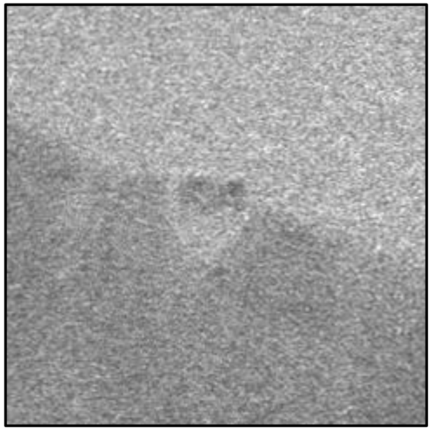

Edge Corrosion of Steel in 0.27 ppm CO_2

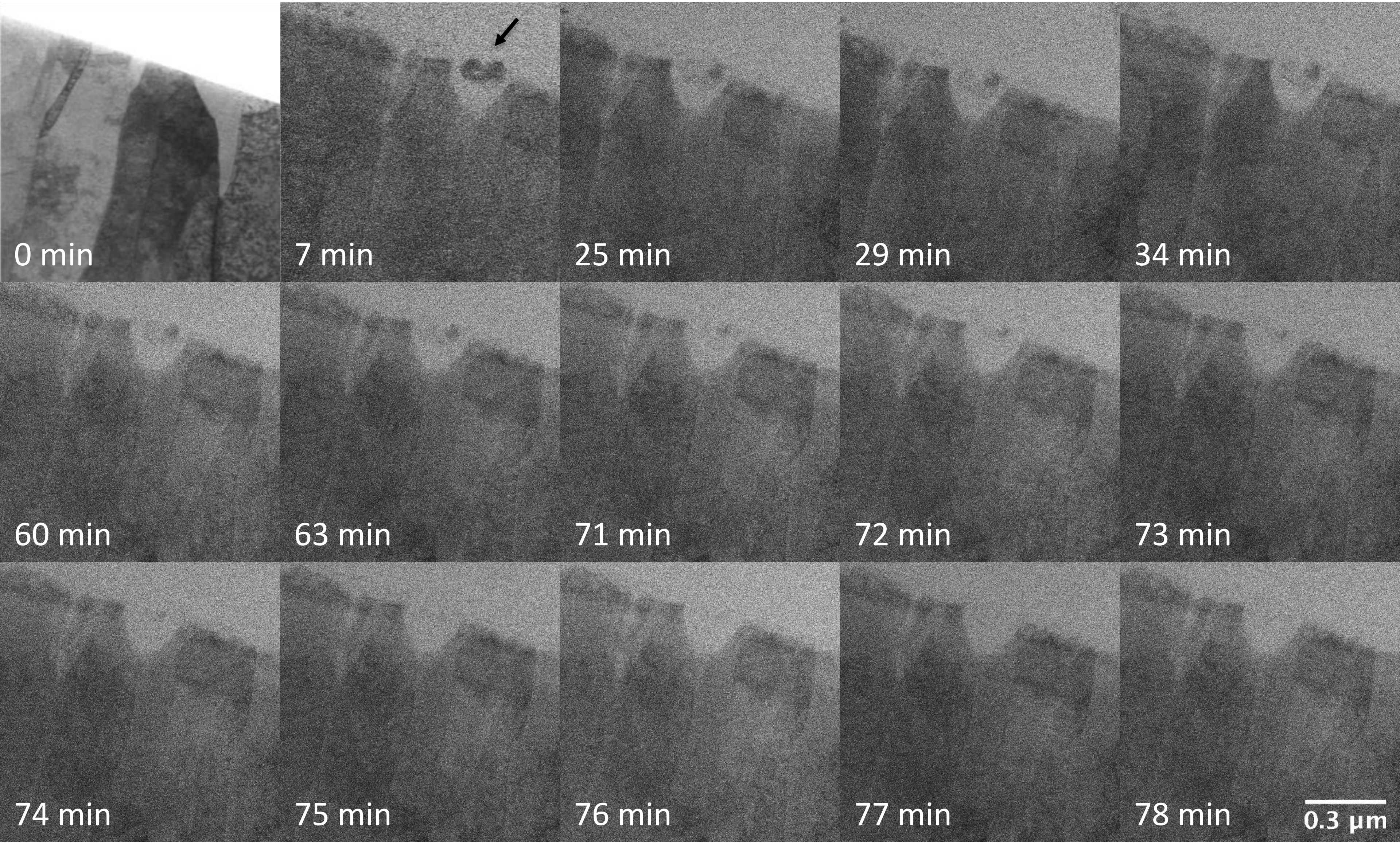

Internal GB Etching of Steel in 0.27 ppm CO_2

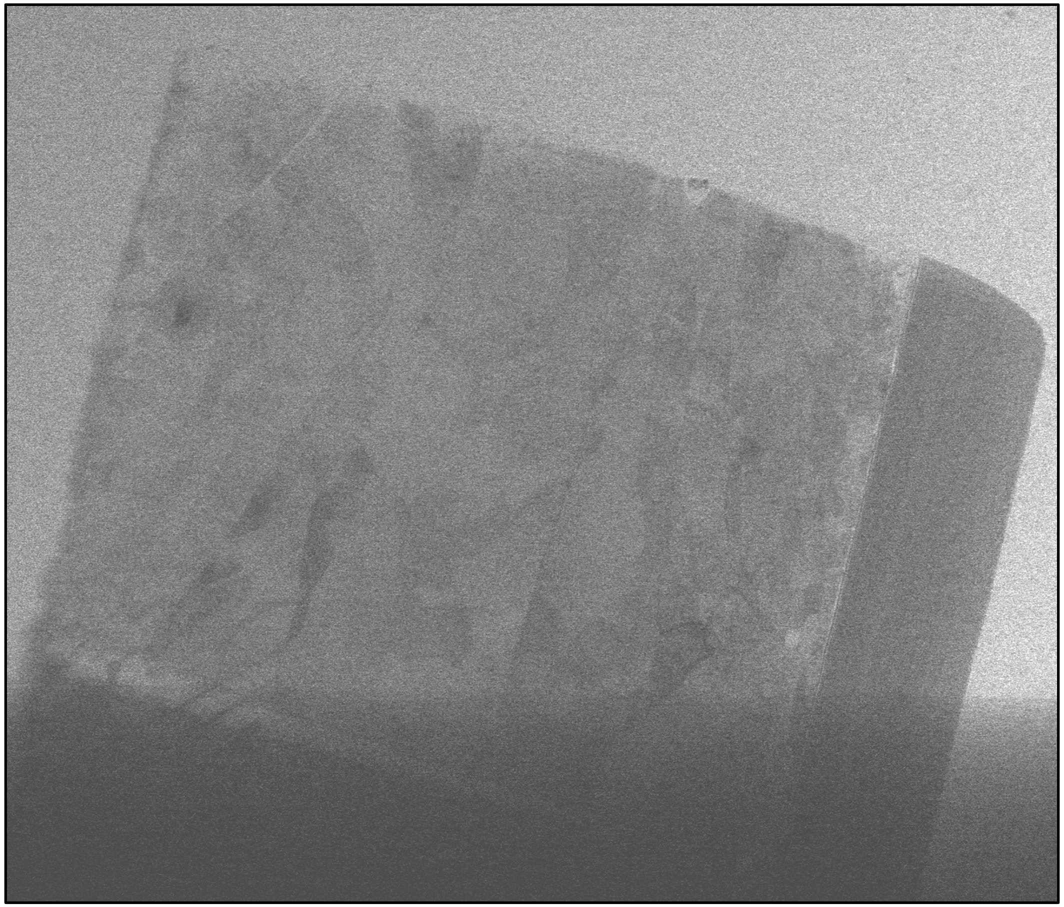

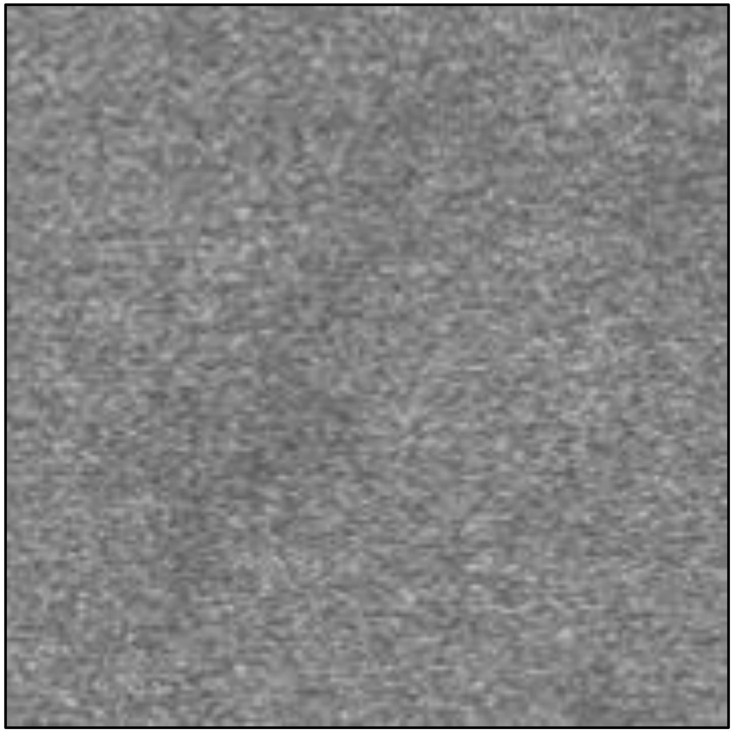

Internal GB Etching of Steel in 0.27 ppm CO_2

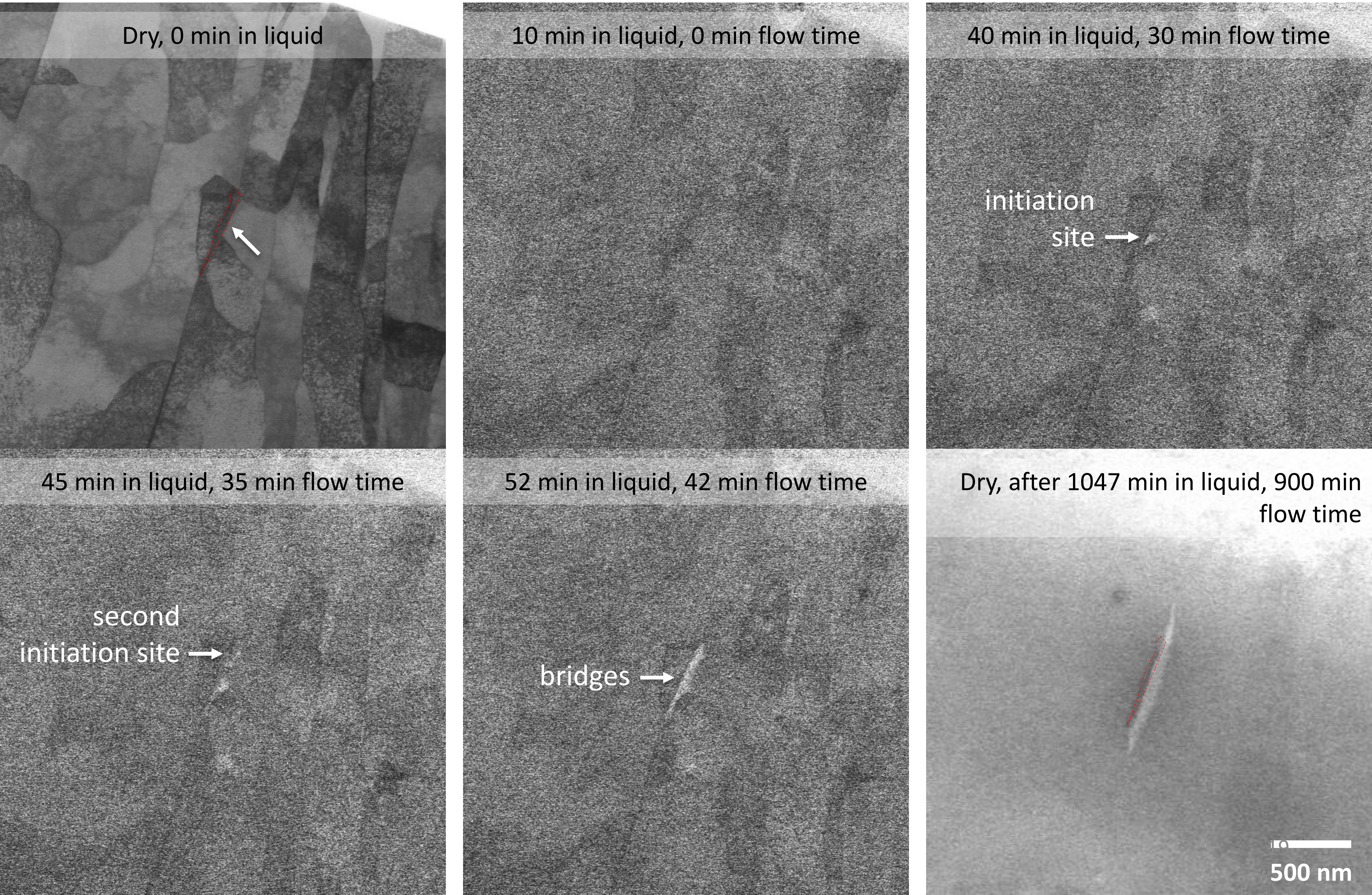

Preferential α-Fe Etching of Steel in 0.27 ppm CO_2

EELS Thickness Measurements After Experiment

Si_3N_4 window = 0.38 IMFP (~49 nm)

Initial sample thickness = 1.61 IMFP (~123 nm Fe)

1. 1.16 IMFP (~77 nm Fe)
2. 0.87 IMFP (~49 nm Fe)
3. 1.22 IMFP (~84 nm Fe)
4. 0.86 IMFP (~47 nm Fe)

Fe_3C/α-Fe thickness ratio=1.67

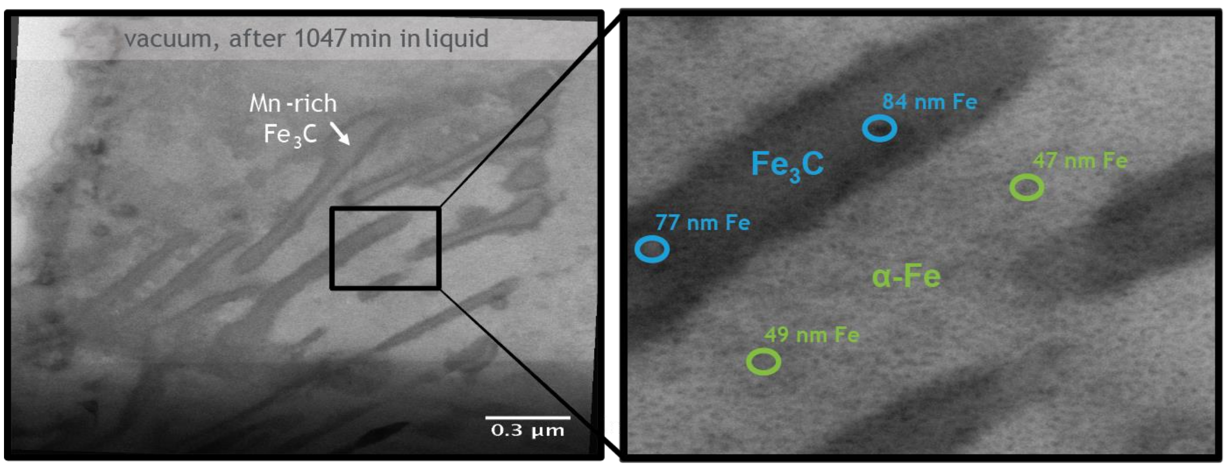

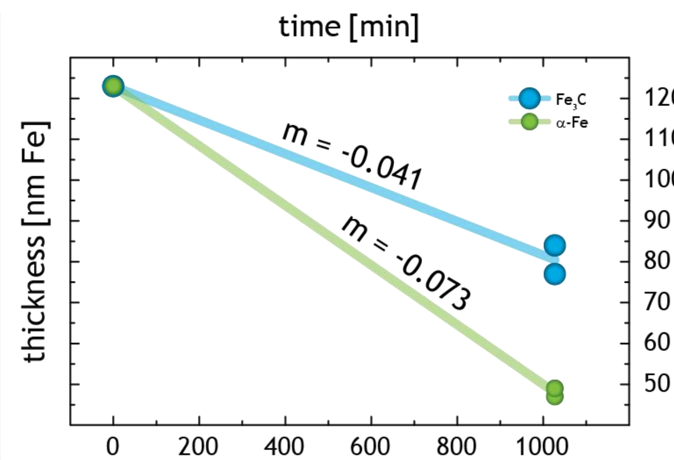

Galvanic Coupling in Low-Carbon Steel

Ferrite and cementite phases in contact with electrolyte solution will experience charge transfer from the ferrite to the cementite, causing dissolution of the Fe ions in the ferrite grains

- Larger grain size of cementite will result in faster etching of ferrite grain

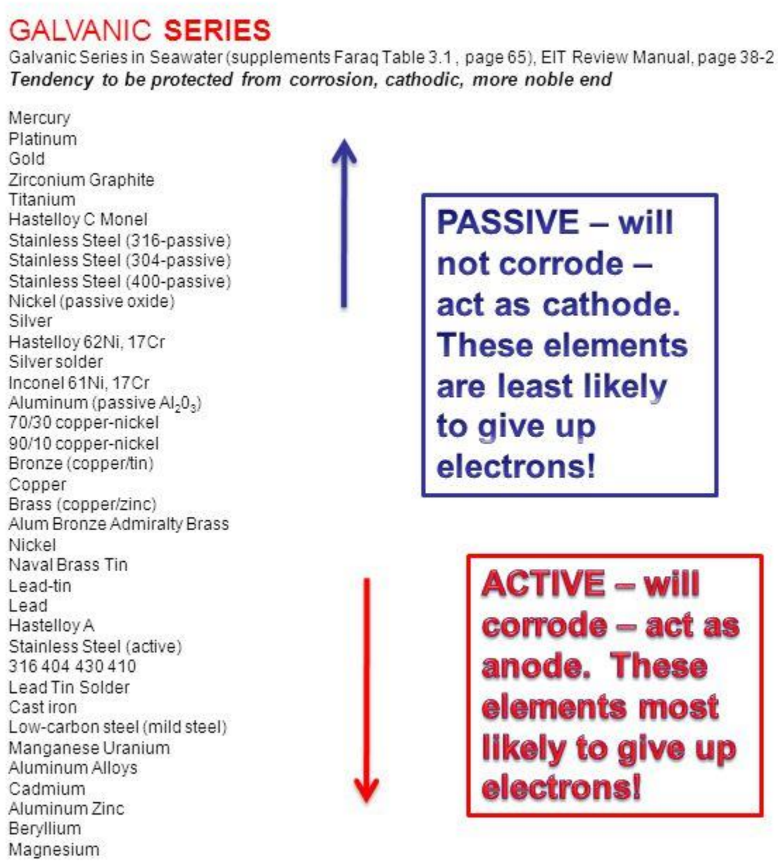

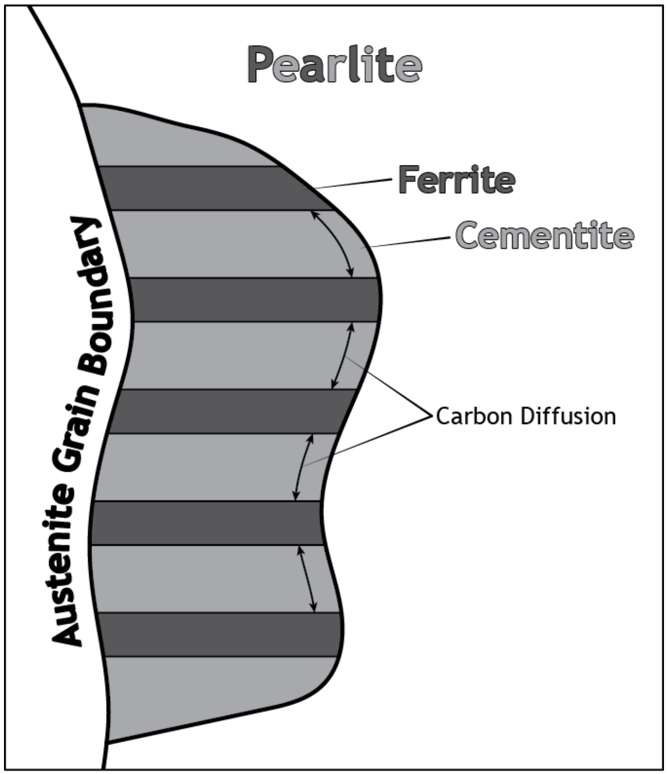

10-20 mV between ferrite and cementite

Pipeline Steel Corrosion: Sour Corrosion H_2S & CO_2

Type of corrosion product controls the corrosion rate
Temperature and partial pressure of H_2S affect the deposition mechanism of film

Polymorphous FeS Corrosion products.

Name	Chemical formula	Crystal structure	Properties
Amorphous	FeS	No specific crystal	Unstable, converts into mackinawite quickly
Mackinawite	$Fe_{1+x}S$ ($x = 0.02–0.41$)	Tetragonal, two- dimensional layer	Metastable, the initial corrosion product
Cubic FeS	FeS	Cubic	Very unstable, can transform into mackinawite, troilite or pyrrhotite
Troilite	FeS	Hexagonal	Stoichiometric end member of the $Fe_{1-x}S$ group ($x = 0$)
Pyrrhotite	$Fe_{1-x}S$ ($x = 0.05–0.21$)	Monoclinic or hexagonal (main)	Thermodynamically stable
Pyrite	FeS_2	Cubic	Thermodynamically stable

Kermani and Morshed, Cri. Rev. Corr. Sci. Eng. **59**, 659 (2003).

Corrosion doesn't occur on top of the scale film, but below it
Wax protective film: diffusion of CO_2 through wax layer

Mechanisms of the Anodic Dissolution of Iron in CO_2-Containing Media[19-20]

Reaction No.	Reaction or Equilibrium	pH < 4	4<pH<5	pH> 5
1a	$HCO_3^- \Leftrightarrow (HCO_3^-)_{ads}$	1a	1a	1b
1b	$CO_2 + (OH^-)_{ads} \Leftrightarrow (HCO_3^-)_{ads}$			
2	$(HCO_3^-)_{ads} \Rightarrow (HCO_3)_{ads} + e^-$	$\Leftrightarrow$	$\Leftrightarrow$	RDS$\Rightarrow$
3	$(HCO_3)_{ads} \Rightarrow (HCO_3^+)_{ads} + e^-$	$\Leftrightarrow$	RDS[A]$\Rightarrow$	$\Rightarrow$
4	$(HCO_3^+)_{ads} + OH^- \Rightarrow (CO_3)_{ads} + H_2O$	RDS$\Rightarrow$	$\Rightarrow$	$\Rightarrow$
5	$Fe - (CO_3)_{ads} + H_2O \Rightarrow Fe^{++} + HCO_3^- + OH^-$	$\Rightarrow$	$\Rightarrow$	$\Rightarrow$
$1 \rightarrow 5$	Tafel slope (mV/log)	60/2 = 30	60/1.5=40	60/0.5= 120
$1 \rightarrow 5$	H^+ reaction order	–2	–1	0
$1 \rightarrow 5$	CO_2 reaction order	1	1	1

[A] RDS = rate-determining step.

Shi et al., Corr. Sci. **102**, 103 (2016).

* H_2S can either accelerate corrosion or reduce by providing a protective film on ferrite (small amounts of H_2S)
* Iron sulfide is more protective than $FeCO_3$

Grain Orientation Mapping of BCC Ferrite

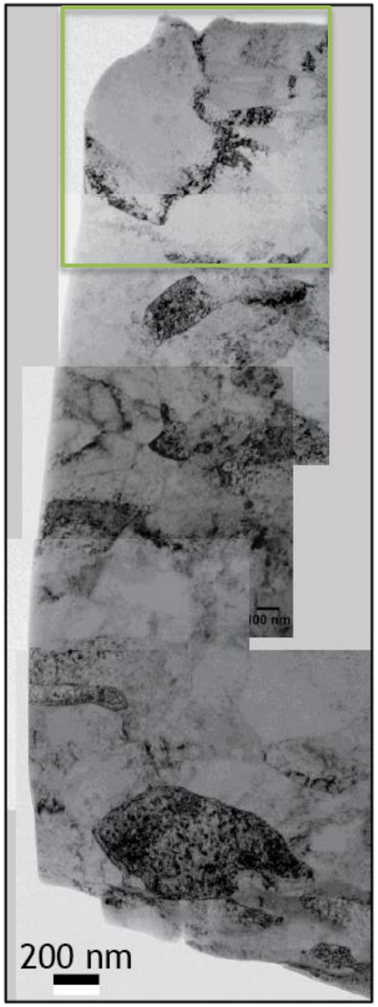

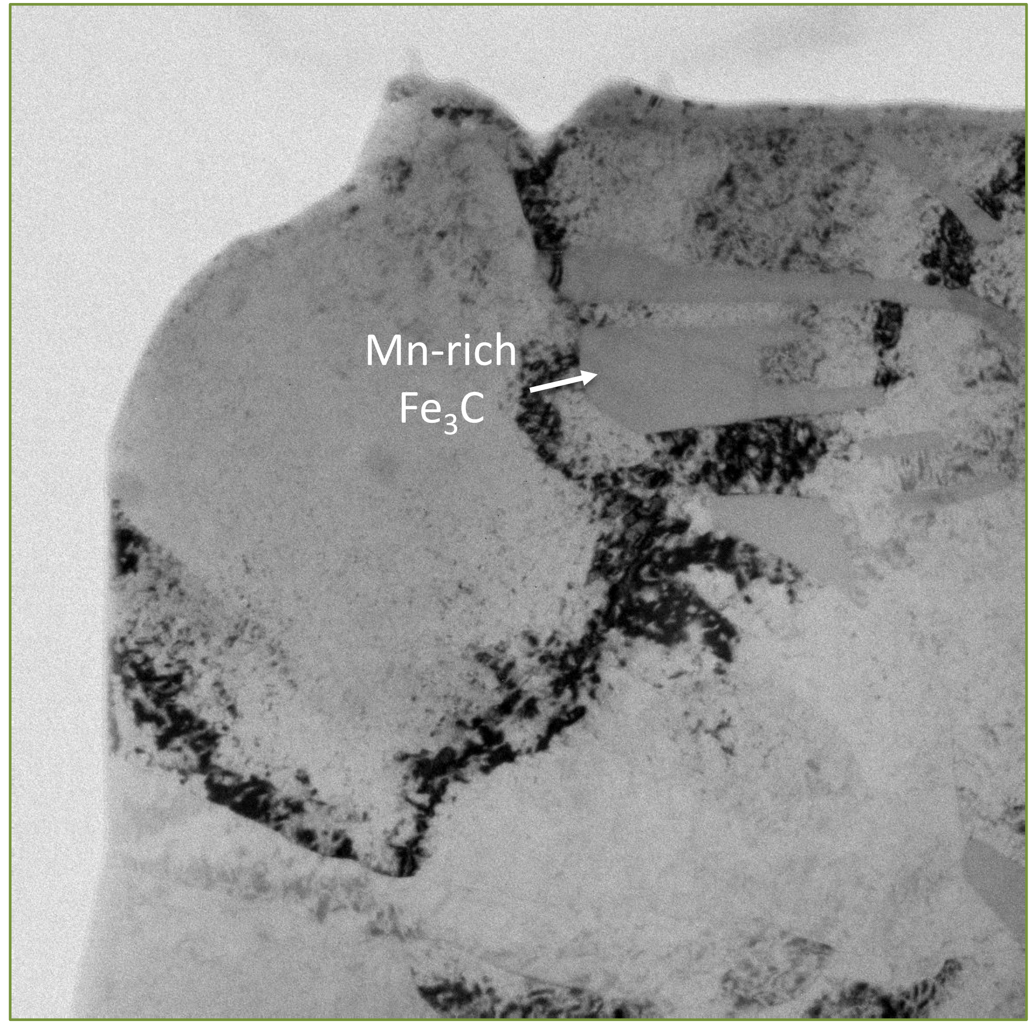

orientation map

Steel in 5 ppm H_2S + 45 ppm CO_2: Microstructural Evolution Overview

- Overall thinning
- White boxes
  - Preferential etching of Fe_3C (over α-Fe)

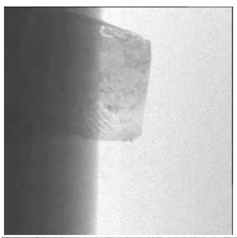

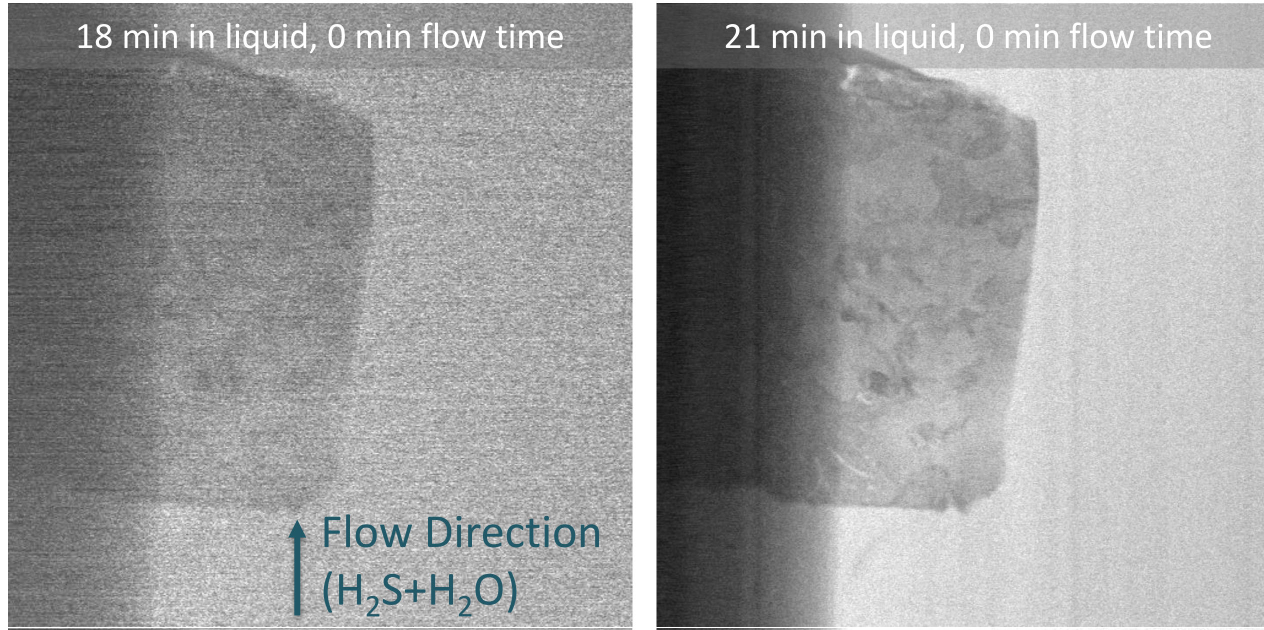

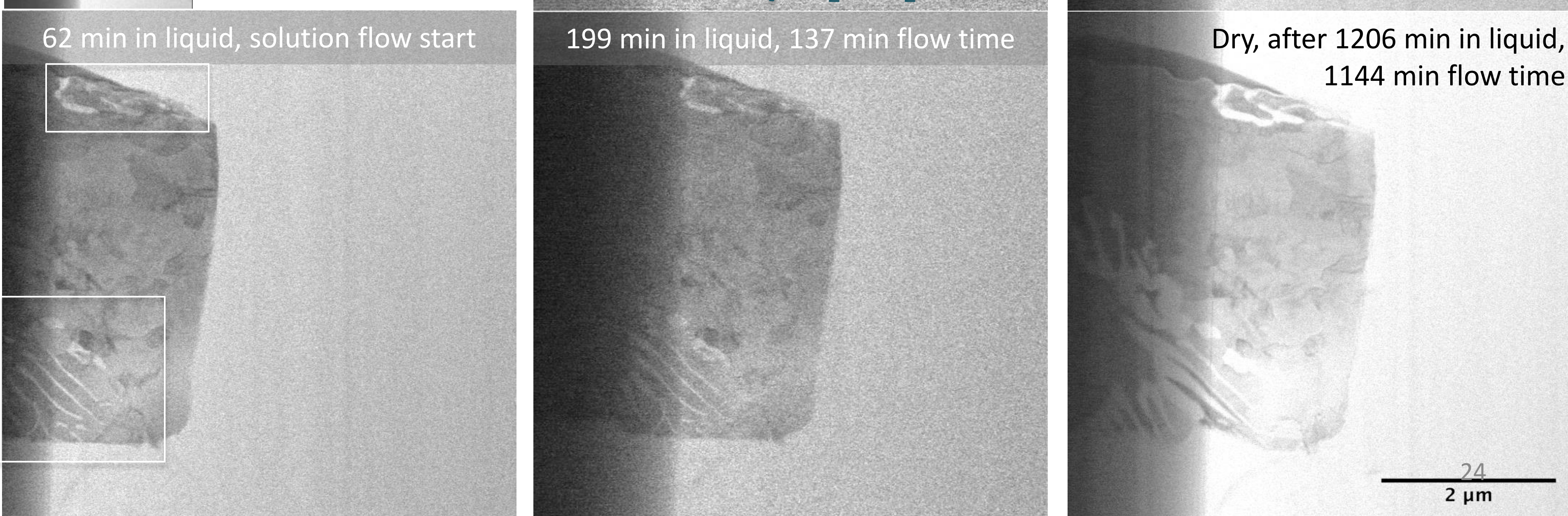

Fe_3C Preferential Etching in 5 ppm H_2S + 45 ppm CO_2

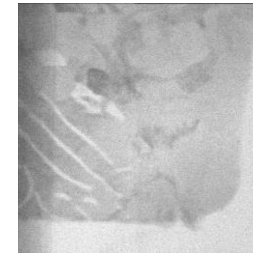

- Lamellar morphology indicates Fe_3C
- Pre-experiment precession diffraction pattern acquired at lamella indicates Fe_3C

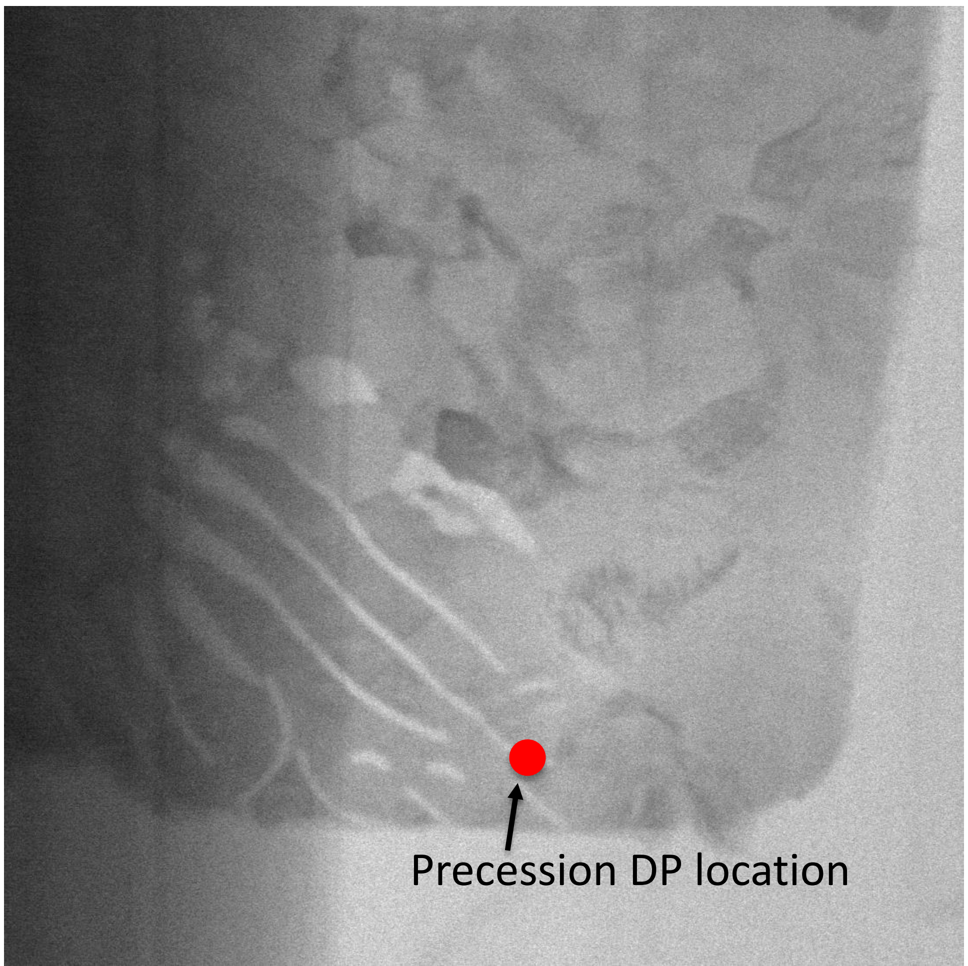

α-Fe [014] ZA
Fe_3C [121] ZA

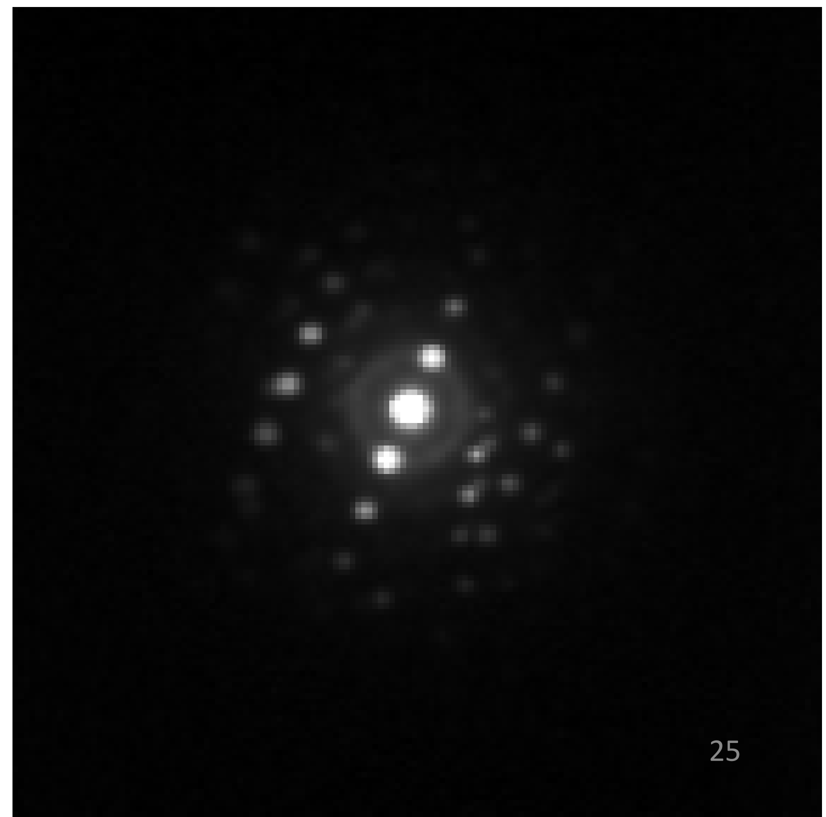

Determination of Scale Products on Surface

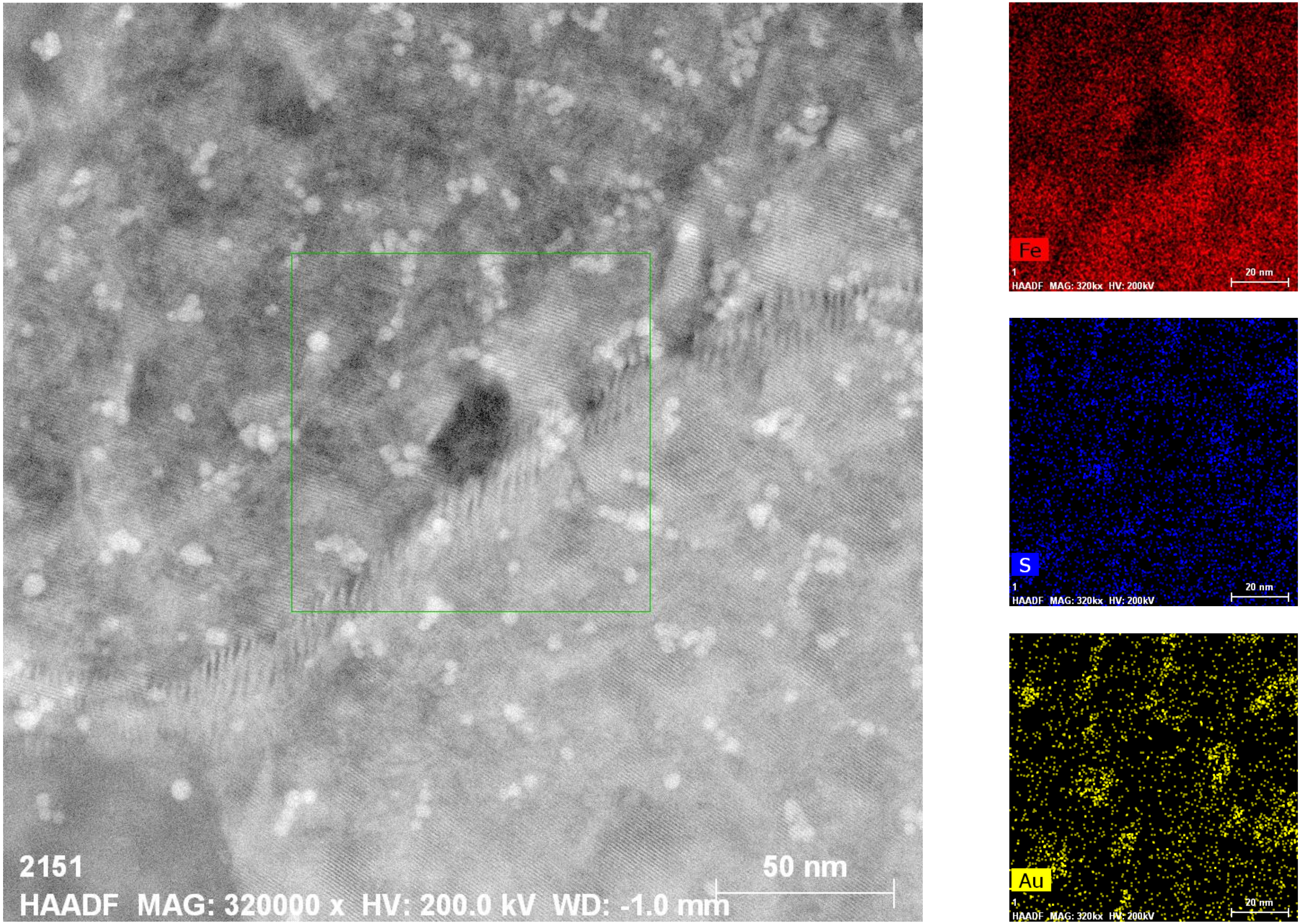

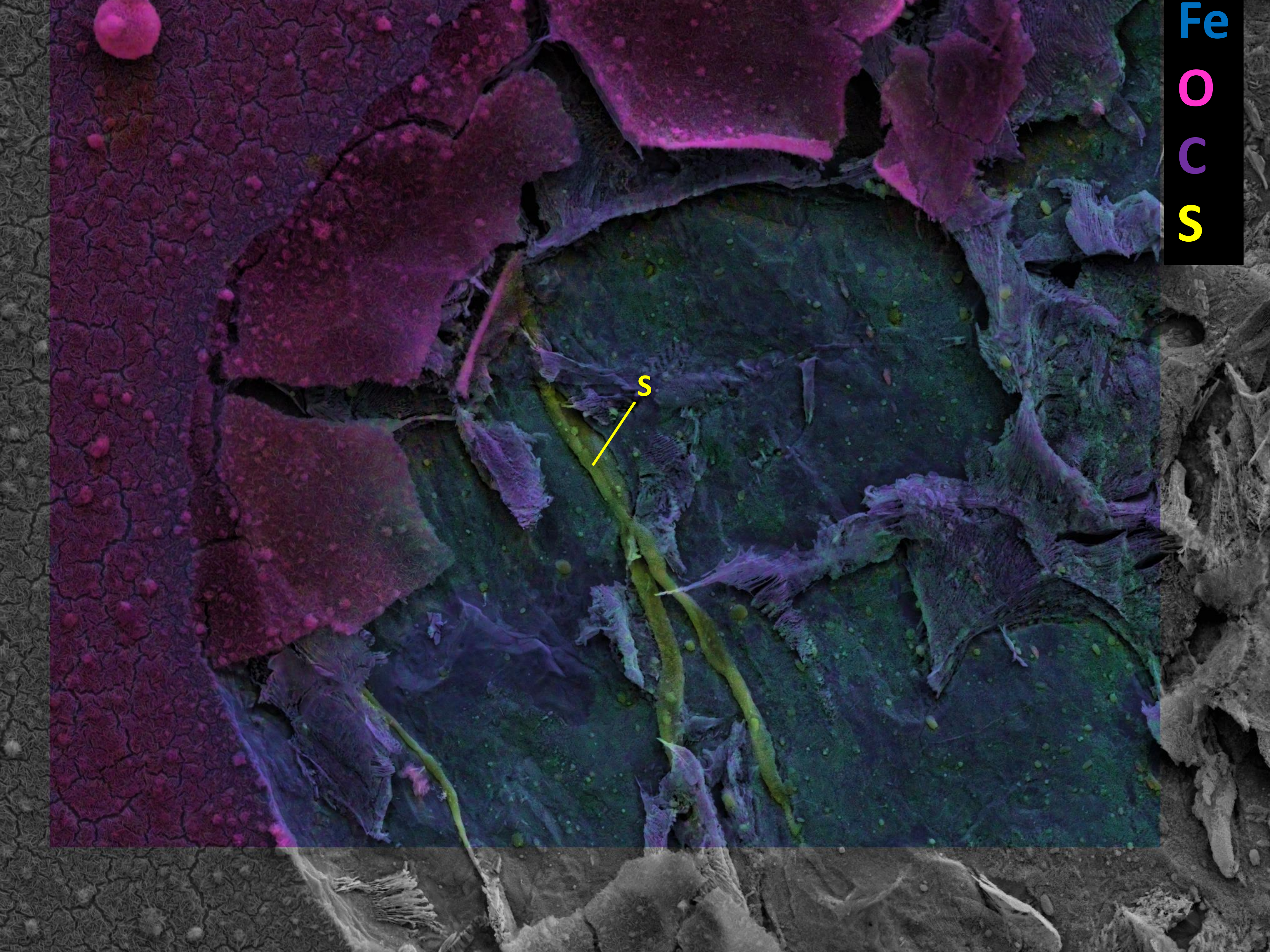
Fe
O
C
S
S

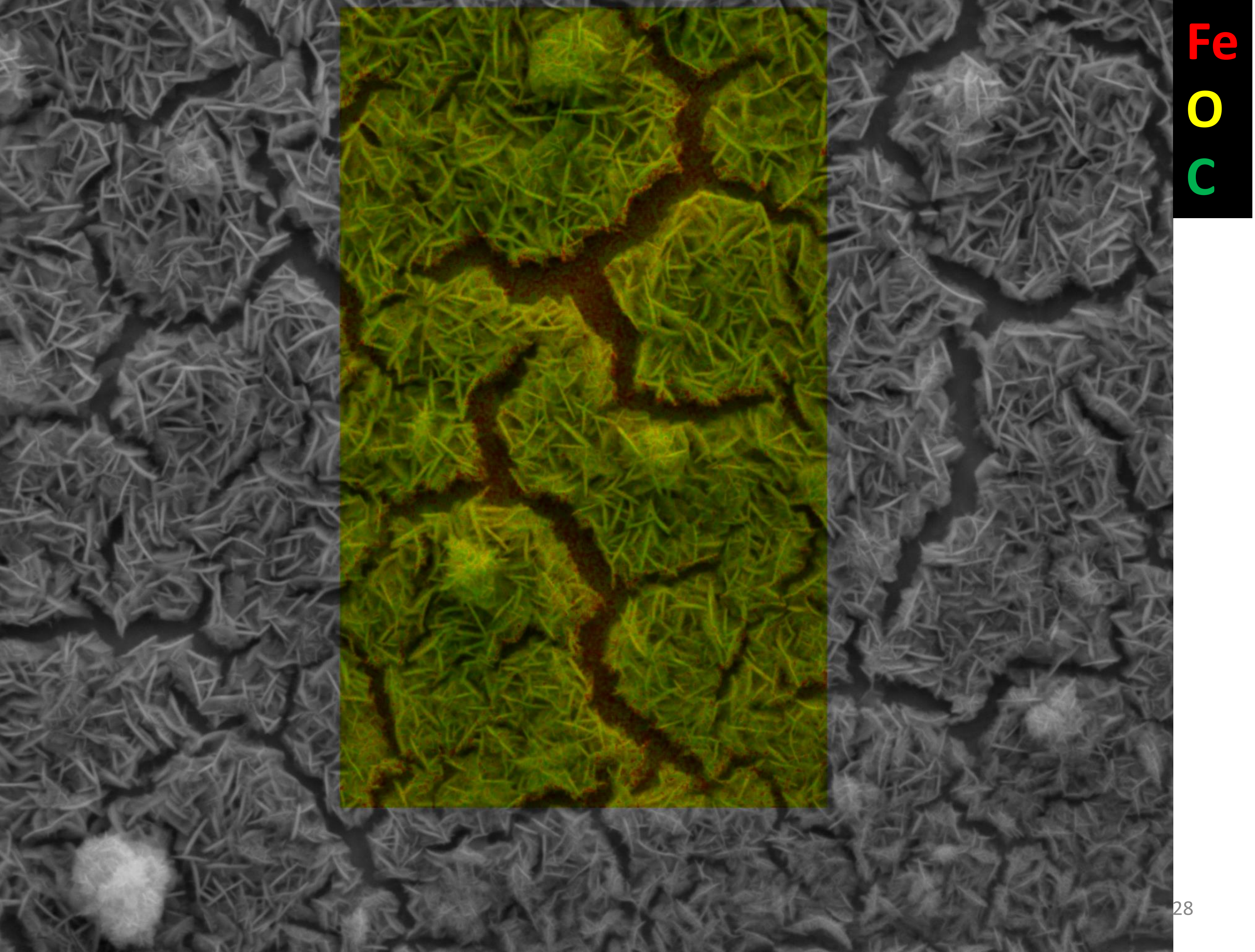
Fe
O
C

Summary of Corrosion Initiation in Low-Carbon Steel

- Sweet: 0.27 ppm CO_2 etches the low-carbon steel
  - Evidence of intergranular corrosion at Fe_3C/α-Fe interface
  - Preferential etching of α-Fe over Fe_3C

- Sour: 5 ppm H_2S with 45 ppm CO_2
  - Fe_3C preferentially etches over α-Fe
    - Unlike the CO_2 only solution

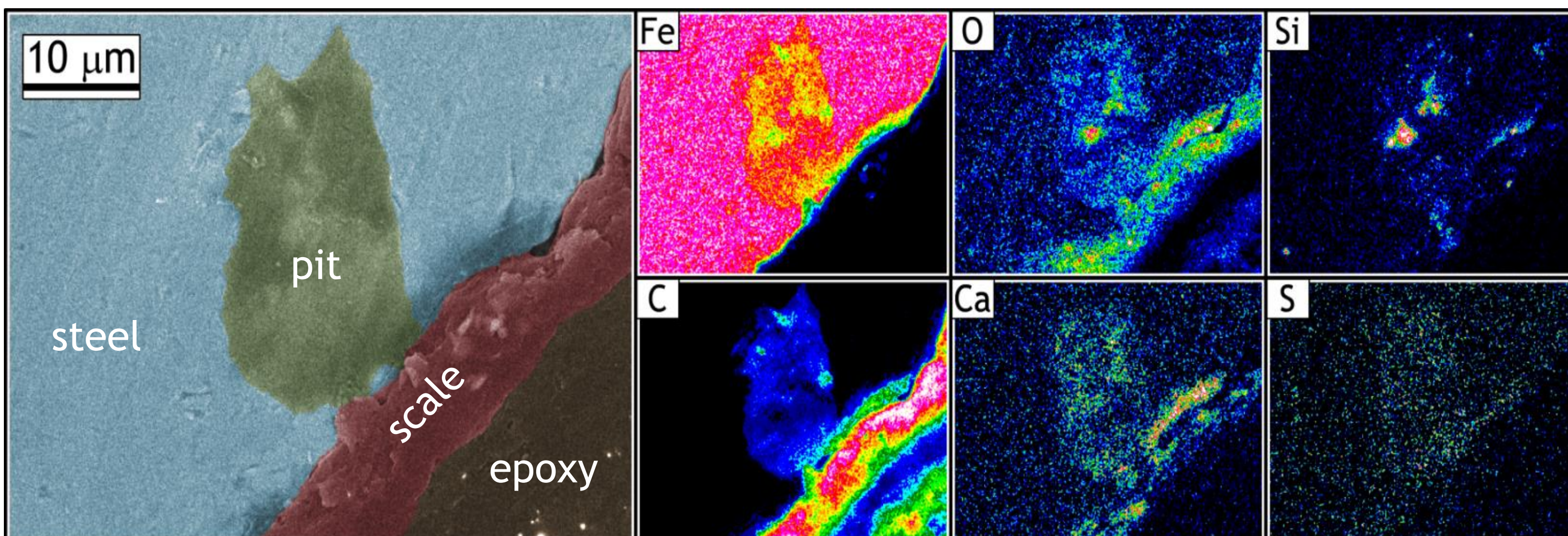

Temperature Dependence of Corrosion

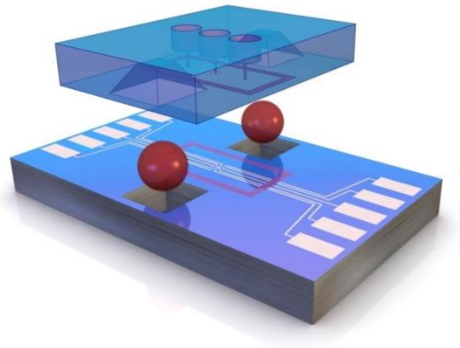

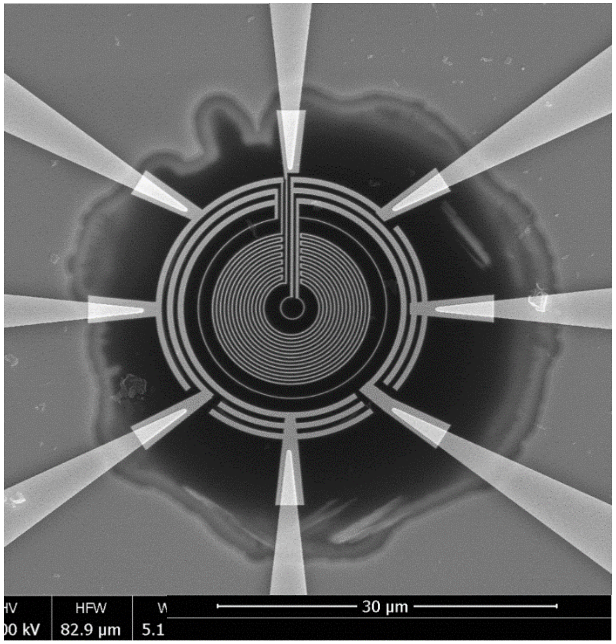

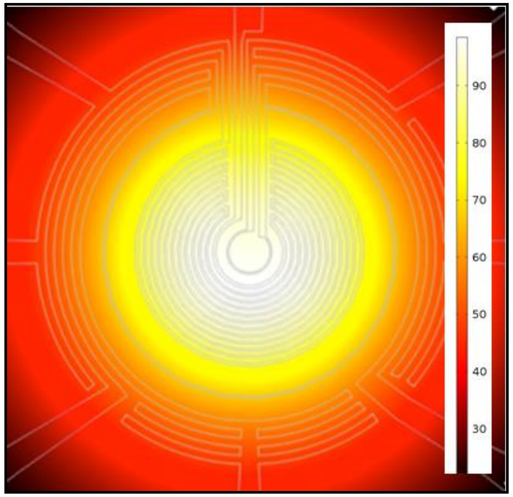

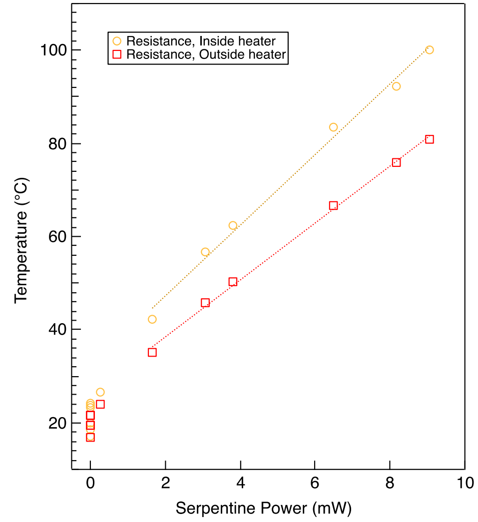

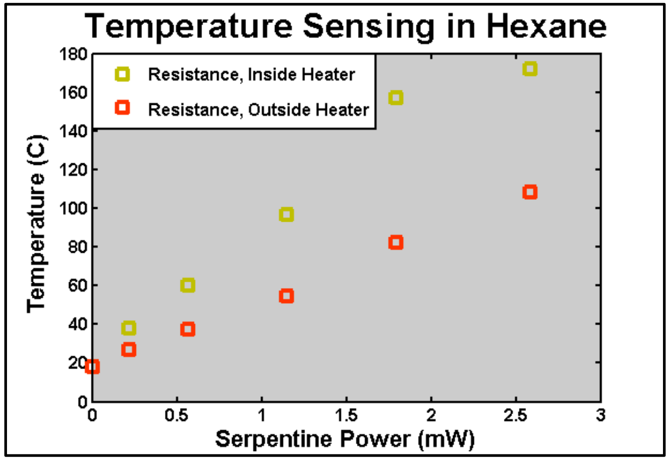

Liquid thickness plays a larger role in heating calibration than the liquid thermal conductivity, therefore measurement of the temperature changes on column is preferable

Center for Integrated Nanotechnologies

CINT Core Facility: Albuquerque, NM

CINT Gateway Facility: Los Alamos, NM

Department of Energy, Basic Energy Sciences national user facility to provide expertise and instrumentation free of charge to support accepted peer-reviewed nanoscience research

Center for Integrated Nanotechnologies CINT Discovery Performance Education Integration Sandia Los Alamos

Sandia National Laboratories

kljungj@sandia.gov

Acknowledgements

Katie

Claire

Steven

Tanya

Tim

Rachael

Michele

aramco

This work was performed, in part, at the Center for Integrated Nanotechnologies (CINT), a U.S. DOE Office of Basic Energy Sciences user facility. Sandia National Laboratories is a multiprogram laboratory managed and operated by Sandia Corporation, a wholly-owned subsidiary of Lockheed Martin Corporation, for the U.S. Department of Energy's National Nuclear Security Administration under contract DE-AC0494AL85000.

Aramco Services Company, Boston MA

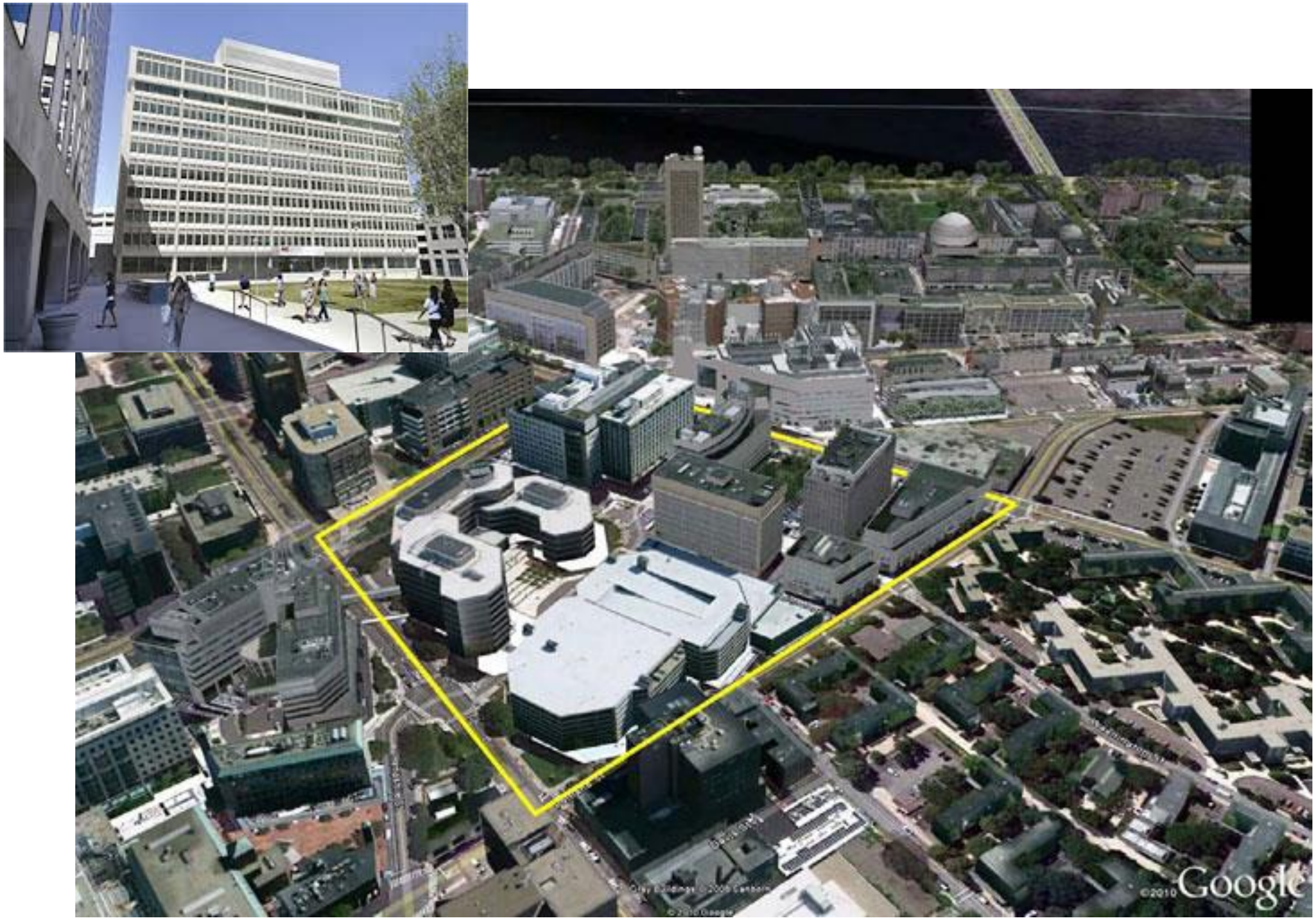

aramco